11-3-2023

In situ profiling reveals metabolic alterations in the tumor microenvironment of ovarian cancer after chemotherapy

Sara Corvigno
University of Texas MD Anderson Cancer Center
Premal H Thaker
Washington University School of Medicine in St. Louis
et al.

ARTICLE OPEN

Check for updates

In situ profiling reveals metabolic alterations in the tumor microenvironment of ovarian cancer after chemotherapy

Sara Corvigno[1], Sunil Badal[2,14], Meredith L. Spradlin[2,14], Michael Keating[2], Igor Pereira[2], Elaine Stur[1], Emine Bayraktar[1], Katherine I. Foster[1], Nicholas W. Bateman[3,4], Waleed Barakat[3,4], Kathleen M. Darcy[3,4], Thomas P. Conrads[3,5], G. Larry Maxwell[3,5], Philip L. Lorenzi[6], Susan K. Lutgendorf[7], Yunfei Wen[1], Li Zhao[8], Premal H. Thaker[9], Michael J. Goodheart[10], Jinsong Liu[11], Nicole Fleming[1], Sanghoon Lee[1], Livia S. Eberlin[12]✉ and Anil K. Sood[1,13]✉

In this study, we investigated the metabolic alterations associated with clinical response to chemotherapy in patients with ovarian cancer. Pre- and post-neoadjuvant chemotherapy (NACT) tissues from patients with high-grade serous ovarian cancer (HGSC) who had poor response (PR) or excellent response (ER) to NACT were examined. Desorption electrospray ionization mass spectrometry (DESI-MS) was performed on sections of HGSC tissues collected according to a rigorous laparoscopic triage algorithm. Quantitative MS-based proteomics and phosphoproteomics were performed on a subgroup of pre-NACT samples. Highly abundant metabolites in the pre-NACT PR tumors were related to *pyrimidine metabolism* in the epithelial regions and *oxygen-dependent proline hydroxylation of hypoxia-inducible factor alpha* in the stromal regions. Metabolites more abundant in the epithelial regions of post-NACT PR tumors were involved in the *metabolism of nucleotides*, and metabolites more abundant in the stromal regions of post-NACT PR tumors were related to *aspartate and asparagine metabolism*, *phenylalanine and tyrosine metabolism*, *nucleotide biosynthesis*, and the *urea cycle*. A predictive model built on ions with differential abundances allowed the classification of patients' tumor responses as ER or PR with 75% accuracy (10-fold cross-validation ridge regression model). These findings offer new insights related to differential responses to chemotherapy and could lead to novel actionable targets.

npj Precision Oncology (2023)7:115 ; https://doi.org/10.1038/s41698-023-00454-0

INTRODUCTION

The standard first-line chemotherapy approach in high-grade serous ovarian cancer (HGSC) has been a combination of taxanes and platinum for over two decades[1]. High overall mortality[2] from HGSC is related to an advanced stage at diagnosis and the rapid emergence of chemotherapy resistance. Mechanisms of resistance, including metabolic changes and adaptation, are not fully understood. Here, we used an innovative strategy to characterize spatially resolved metabolic changes in a highly clinically annotated set of HGSC samples collected before and after neoadjuvant chemotherapy (NACT) from patients treated consistently according to a surgical algorithm[3].

Mass spectrometry (MS) is a powerful technology to spatially characterize the molecular composition of tissues within the tumor microenvironment (TME)[4–8]. We employed desorption electrospray ionization (DESI)-MS, which allows the simultaneous detection of diverse metabolites and lipid species directly from native tissues under ambient conditions[9,10]. The use of histologically compatible spray solvents allows for the same tissue sections to be stained with hematoxylin and eosin (H&E) to visualize tissue morphology[11]. To corroborate metabolic findings with molecular data, we performed global proteomics and phosphoproteomics using laser capture (LC)-MS. These results provide new insights into the metabolic alterations in the tumor and stromal compartments based on response to NACT.

RESULTS

Metabolic profiling of pre-chemotherapy tumor tissues using DESI-MS

We first used DESI-MS on pre-NACT tissues from patients stratified as having excellent response (ER) or poor response (PR) to NACT (Supplementary Table 1). MS imaging data were extracted from the epithelial and stromal regions following manual segmentation (Fig. 1). A preliminary analysis on reproducibility was performed where two sections from the same tumor (one mouse xenograft and two human ovarian cancer samples) were analyzed with DESI-MS (Supplementary Fig. 1A) and a cosine similarity test was performed, yielding a score of 0.981 for mouse xenograft (Supplementary Fig. 1B) and 0.998 (Supplementary Fig. 1C) and 0.968 (not shown) for human tumors. In addition, four sections from 4 mouse xenografts were analyzed with an average cosine score of 0.972 (Supplementary Fig. 1D). Manual segmentation allowed us to distinguish between epithelial and stromal areas;

[1]Department of Gynecologic Oncology and Reproductive Medicine, The University of Texas MD Anderson Cancer Center, Houston, TX, USA. [2]Department of Chemistry, The University of Texas at Austin, Austin, TX, USA. [3]Gynecologic Cancer Center of Excellence, Department of Gynecologic Surgery and Obstetrics, Uniformed Services University of the Health Sciences, Walter Reed National Military Medical Center, Bethesda, MD, USA. [4]The Henry M. Jackson Foundation for the Advancement of Military Medicine, Inc., Bethesda, MD, USA. [5]Women's Health Integrated Research Center, Women's Service Line, Inova Health System, Falls Church, VA, USA. [6]Department of Bioinformatics and Computational Biology, The University of Texas MD Anderson Cancer Center, Houston, TX, USA. [7]Departments of Psychological and Brain Sciences, Obstetrics and Gynecology, and Urology, University of Iowa, Iowa City, IA, USA. [8]Department of Genomic Medicine, The University of Texas MD Anderson Cancer Center, Houston, TX, USA. [9]Department of Obstetrics and Gynecology, Division of Gynecologic Oncology, Washington University, St. Louis, MO, USA. [10]Department of Obstetrics and Gynecology, Division of Gynecologic Oncology, University of Iowa, Iowa City, IA, USA. [11]Department of Anatomic Pathology, The University of Texas MD Anderson Cancer Center, Houston, TX, USA. [12]Department of Surgery, Baylor College of Medicine, Houston, TX, USA. [13]Center for RNA Interference and Non-Coding RNA, The University of Texas MD Anderson Cancer Center, Houston, TX, USA. [14]These authors contributed equally: Sunil Badal, Meredith L. Spradlin. ✉email: Livia.Eberlin@bcm.edu; asood@mdanderson.org

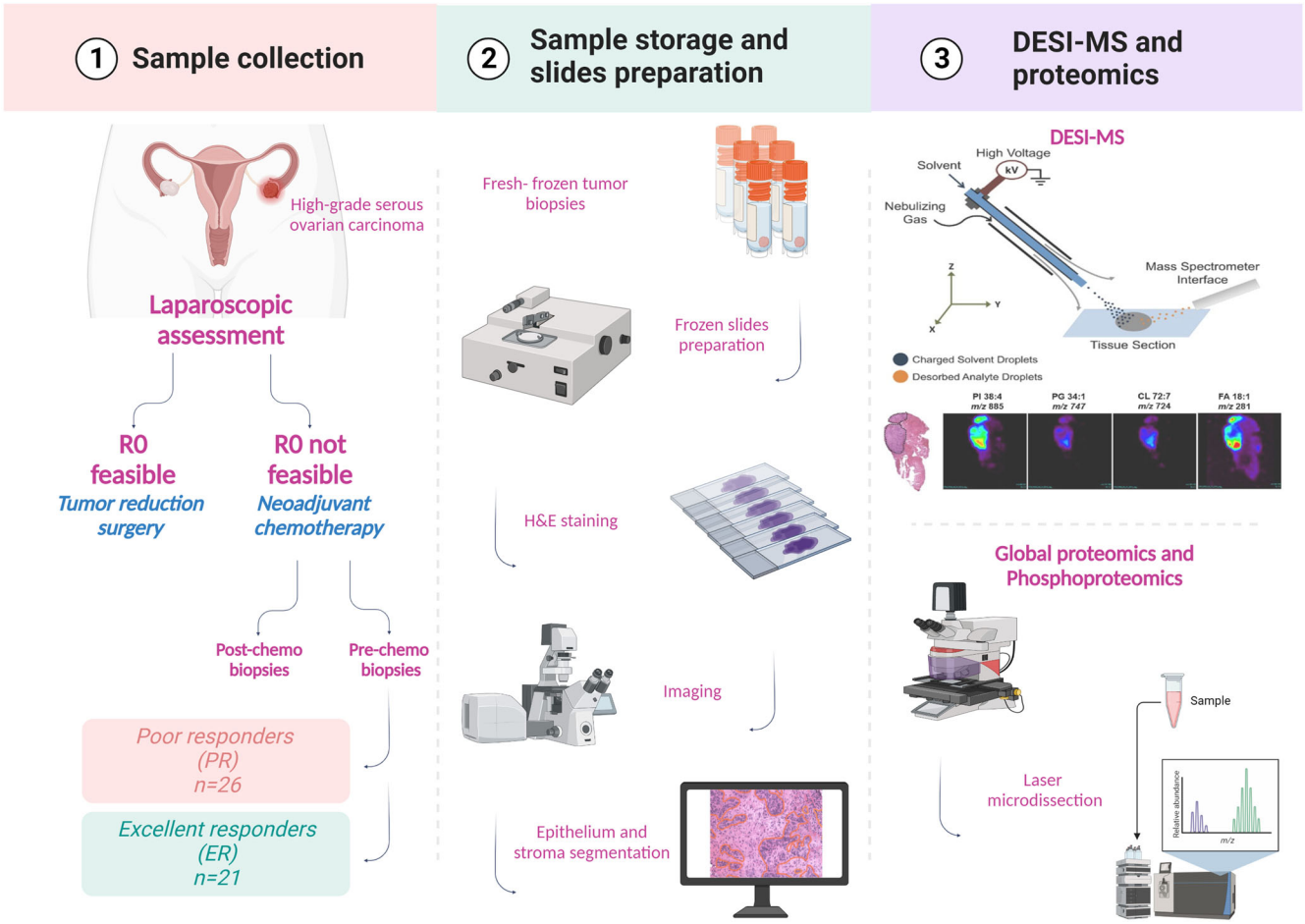

Fig. 1 Graphical abstract. R0 absence of macroscopic residual at surgery, ER excellent responders, PR poor responders.

the resolution of the technique does not allow for single cell-level segmentation. Stromal regions were mostly characterized by fibroblast-like cells and extracellular matrix (e.g., elastic fibers) that can be identified with H&E stain. Necrotic areas were excluded. Representative DESI-MS images of nine metabolites for two PR and ER tissues are shown in Fig. 2a. We employed negative ion mode DESI-MS imaging to detect small molecules, such as sugars, nucleotides, and amino acids, and a vast range of lipid classes. Multiple lipids, such as fatty acids, monoacylglycerols, ceramides, cardiolipins, and phospholipids, showed different relative abundances between ER and PR tissues. Significance analysis of microarrays (SAM) revealed that the epithelial regions of PR samples, as compared to those of ER samples, had significantly higher relative abundances of fatty acids, phosphatidic acids, ceramides, cardiolipins, and monoacylglycerols; the stromal regions of PR samples had higher relative abundances of fatty acids and phosphatidic acids (Table 1 and Fig. 2b) as compared to those of ER samples. A number of small molecules were also detected in both the ER and PR samples (Fig. 2c); SAM revealed that several molecules had significantly higher relative abundances in the epithelial PR samples than in the epithelial ER samples. In particular, hydroxybutyric acid and ubiquinone were detected at significantly higher relative abundances in the ER samples, while taurine and uridine were detected at significantly higher relative abundances in the PR samples. The stromal regions of the ER samples had significantly higher relative abundances of hydroxybutyric acid, hexose, and uridine, while metabolites with significantly higher abundances in the PR stroma samples included succinic acid and taurine (Table 1).

To investigate if the small metabolites whose relative abundances significantly differed between ER and PR tumors were associated with specific metabolic pathways, we used two publicly available software programs. These programs analyzed the metabolites with higher or lower relative abundances in the different cohorts and tissues and provided the metabolic pathways in which such metabolites are particularly enriched. Taurine and uridine (Table 1B), which were detected at higher relative abundances in the epithelium of PR samples, mapped mainly to the “recycle of bile acids and salts” pathway (FDR-adjusted $p < 0.05$) and the “pyrimidine salvage and catabolism” pathway (FDR-adjusted $p < 0.05$) (Supplementary Table 2A, B). In contrast, the metabolites hydroxybutyric acid and ubiquinone (Table 1A), which had higher relative abundance in the epithelial regions of ER samples, showed a correlation with the “respiratory electron transport” and “metabolism of amino acids and derivatives” pathways (FDR-adjusted $p < 0.05$) (Supplementary Table 3A).

In the stromal regions of the pre-chemotherapy tissues, hydroxybutyric acid, hexose, asp-his, and uridine, which were detected at higher relative abundances in ER samples (Table 1C), were associated with several pathways, including the “pyrimidine salvage” pathway (Supplementary Table 4A, B, Table 2A). The metabolites succinic acid and taurine (Table 1D), which had higher abundances in PR tumors, were related to the “transport of bile salts and organic acids metal ions and amine compounds” and ”oxygen-dependent proline hydroxylation of hypoxia-inducible factor alpha” pathways (FDR-adjusted $p < 0.05$ for both) (Supplementary Table 5A, B, Table 2A). Table 2A summarizes the

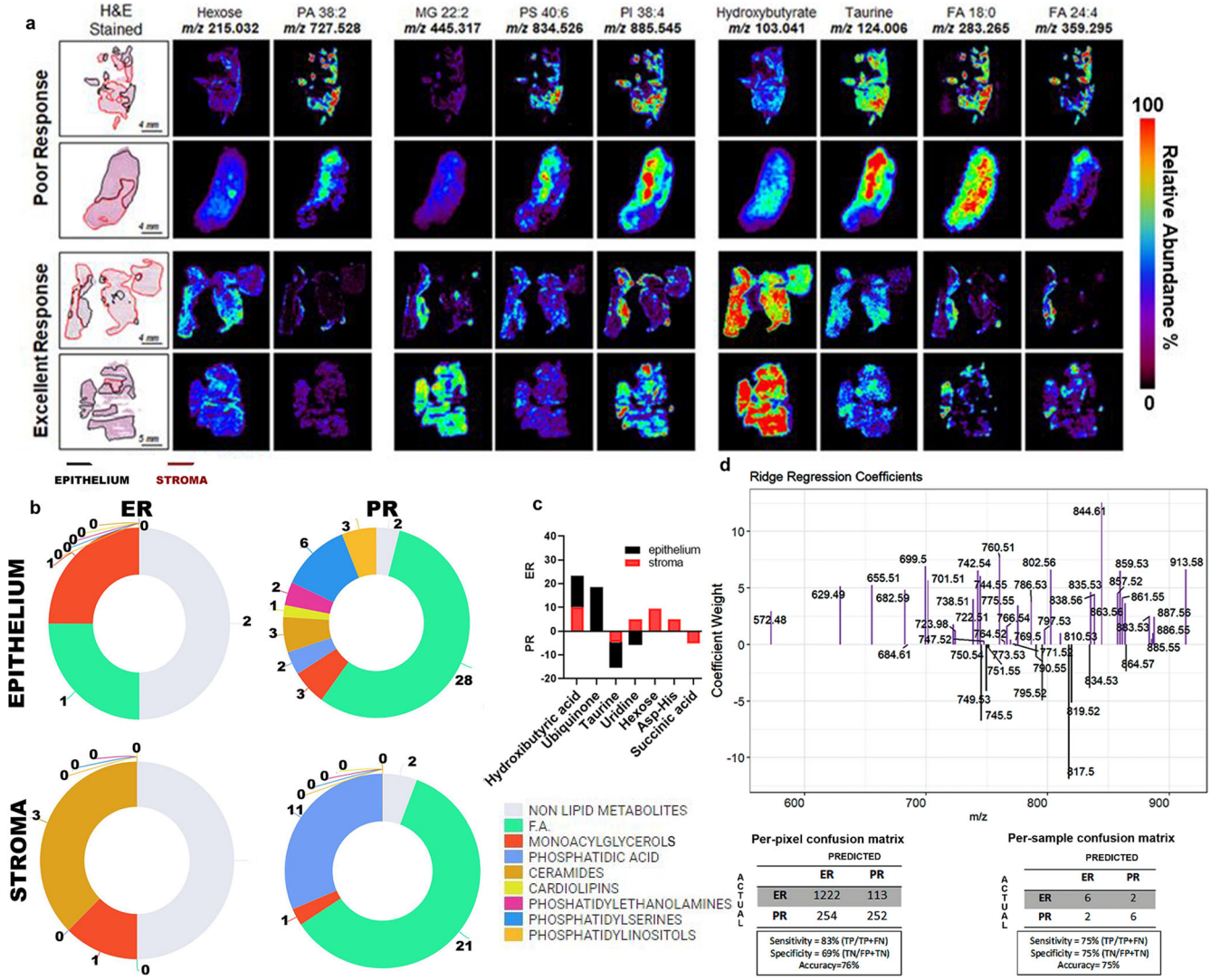

Fig. 2 Analysis of high-grade serous ovarian cancer (HGSC) samples obtained prior to neoadjuvant chemotherapy (NACT) based on excellent (ER) or poor (PR) response. a DESI-MS imaging of tumor tissue sections obtained from 52 patients (30 ER and 22 PR) was performed. Negative ion mode DESI-MS ion images of two ER and two PR tumors showing the spatial distribution and relative abundances of nine metabolites and lipid species for each sample are represented. Within each column, the ion images were normalized to the same ion intensity (100% relative abundance, red) for ease of comparison among individual samples and response groups. Optical images of the H&E-stained tissue sections are shown for each sample, with regions of tumor epithelium outlined in black and regions of stroma outlined in red. b Distribution of lipid classes representing higher relative abundances in the stroma and epithelium of ER and PR pre-chemotherapy tissues, from DESI-MS. c Histograms representing relative abundances of small metabolites in the epithelium and stroma of ER and PR tumors. d Plots of ridge regression coefficients for the predictive model. The analysis was restricted to the primary tumor sites (adnexa and ovaries, N = 16), and samples from metastatic sites (omentum or abdominal organs) were excluded (N = 36). A ridge regression model was used to estimate the probability of every mass spectrum belonging to either the ER or PR group. ER excellent responders, PR poor responders.

pathways related to the detected metabolites that may be altered in pre-chemotherapy ER and PR tissue samples.

Next, we built a predictive model based on the DESI-MS data extracted from the pre-NACT samples from the ER and PR groups acquired from tumor primary sites ($N = 16$). This model predicted response to chemotherapy using cross-validation with a per-pixel sensitivity of 83%, specificity of 69%, and total accuracy of 76%, with a positive predictive value of 92% (Fig. 2d). When the predictive performance per patient was analyzed, sensitivity, specificity, and accuracy values of 75% were achieved.

Metabolic profiling of post-chemotherapy tumor tissues

Next, we analyzed the matched post-chemotherapy tissues from ER and PR tumors and examined the metabolic changes occurring in response to chemotherapy. Discriminant analysis using the sparse partial least squares algorithm was used to identify and plot the most discriminative features[12]. When the epithelial areas of matched pre- and post-NACT tissues were analyzed, the number of metabolic species with lower relative abundances after chemotherapy (as compared to pre-chemotherapy) was higher in ER tumors than in PR tumors. Specifically, 113 metabolites (small molecules and lipids) had lower relative abundances in the epithelial areas of post-NACT tissues of ER tumors, while 65 metabolic species had higher relative abundances in the epithelial areas of post-NACT tissues of ER tumors (SAM, FDR $p < 0.01$) (Table 3A, B). In the epithelial areas of PR tumors, 60 metabolic species showed lower relative abundances in post-NACT tissues, while 45 metabolic species showed higher relative abundances in post-

Table 1. Attribution of compounds for pre-chemotherapy tumors (DESI-MS imaging acquired in the negative ion mode; attributions were assigned based on high mass accuracy and MS/MS measurements).

A. Compounds identified by SAM as relatively more abundant in ER (excellent responders) compared to PR (poor responders) samples. Data were extracted from epithelial regions.

Tentative attribution	Molecular formula	Detected *m/z*	Mass error (ppm)	SAM score	KEGG ID
Metabolites					
Hydroxybutyric acid	$C_4H_7O_3$	103.0404	−3.0	13.254	C05984
Ubiquinone	$C_{29}H_{41}O_4$	453.3030	−2.3	18.495	C11378
Fatty acids (FA)					
FA 21:1; O	$C_{21}H_{39}O_5$	371.2807	−1.0	7.452	
Monoacylglycerols (MG)					
MG 22:2	$C_{25}H_{46}O_4Cl$	445.3174	−4.2	10.518	

B. Compounds identified by SAM as relatively less abundant in ER compared to PR samples. Data were extracted from epithelial regions.

Tentative attribution	Molecular formula	Detected *m/z*	Mass error (ppm)	SAM score
Metabolites				
Taurine	$C_2H_6NO_3S$	124.0078	−1.7	−10.640
Uridine	$C_9H_{12}N_2O_6Cl$	279.0385	1.4	−5.833
Fatty acids (FA)				
FA 10:0	$C_{10}H_{19}O_2$	171.1387	2.3	−5.678
FA 12:2	$C_{12}H_{19}O_2$	195.1394	1.5	−5.146
FA 14:0	$C_{14}H_{27}O_2$	227.2019	−0.9	−6.750
FA 15:4	$C_{15}H_{21}O_2$	233.1550	1.3	−6.450
FA 15:0	$C_{15}H_{29}O_2$	241.2176	1.2	−9.989
FA 16:1	$C_{16}H_{29}O_2$	253.2179	2.4	−4.239
FA 16:0	$C_{16}H_{31}O_2$	255.2332	0.8	−9.877
FA 17:1	$C_{17}H_{31}O_2$	267.2331	0.4	−5.638
FA 17:0	$C_{17}H_{33}O_2$	269.2488	0.7	−7.161
FA 18:3	$C_{18}H_{29}O_2$	277.2174	0.4	−7.261
FA 18:2	$C_{18}H_{31}O_2$	279.2336	2.3	−6.531
FA 18:1	$C_{18}H_{32}O_2$	281.2493	2.5	−5.851
FA 18:0	$C_{18}H_{35}O_2$	283.2648	1.9	−9.898
FA 20:3	$C_{20}H_{33}O_2$	305.2469	−5.6	−4.224
FA 20:2	$C_{20}H_{35}O_2$	307.2628	−4.9	−7.848
FA 20:1	$C_{20}H_{37}O_2$	309.2795	2.3	−6.736
FA 20:0	$C_{20}H_{39}O_2$	311.2954	−0.6	−8.123
FA 18:1	$C_{18}H_{34}O_2Cl$	317.2256	0.9	−5.735
FA 22:6	$C_{22}H_{31}O_2$	327.2326	1.2	−4.395
FA 22:3	$C_{22}H_{37}O_2$	333.2794	1.5	−6.475
FA 22:2	$C_{22}H_{39}O_2$	335.2957	0.3	−9.145
FA 22:1	$C_{22}H_{41}O_2$	337.3117	1.5	−6.872
FA 24:2	$C_{24}H_{43}O_2$	363.3267	−0.6	−9.104
FA 24:1	$C_{24}H_{45}O_2$	365.3427	0.5	−6.978
FA 24:0	$C_{24}H_{47}O_2$	367.3586	1.2	−5.353
FA 26:2	$C_{26}H_{47}O_2$	391.3579	−0.8	−11.433
FA 26:1	$C_{26}H_{49}O_2$	393.3738	0.0	−10.034
FA 26:0	$C_{26}H_{51}O_2$	395.3896	0.3	−5.498
Monoacylglycerols (MG)				
MG 18:2	$C_{21}H_{38}O_4Cl$	389.2468	1.0	−9.014
MG 18:1	$C_{21}H_{40}O_4Cl$	391.2623	0.5	−4.708
MG 20:4	$C_{23}H_{38}O_4Cl$	413.2467	0.7	−7.177

Table 1 continued

B. Compounds identified by SAM as relatively less abundant in ER compared to PR samples. Data were extracted from epithelial regions.

Tentative attribution	Molecular formula	Detected *m/z*	Mass error (ppm)	SAM score
Ceramides (Cer)				
Cer d34:1	$C_{34}H_{67}NO_3Cl$	572.4797	3.1	−10.403
Cer d42:2	$C_{42}H_{81}NO_3Cl$	682.5891	2.9	−9.818
Cer d42:1	$C_{42}H_{81}NO_3Cl$	684.6070	0.4	−4.100
Phosphatidic acids (PA)				
PA 34:1	$C_{37}H_{70}O_8P$	673.4795	−2.8	−5.278
PA 41:6	$C_{44}H_{74}O_8P$	761.5131	0.5	−4.560
Cardiolipins				
CL 72:7	$C_{81}H_{142}O_{17}P_2$	724.4836	−4.3	−7.918
Phosphatidylethanolamines				
PE 34:4	$C_{39}H_{69}NO_8P$	710.4752	−2.0	−4.842
PE 38:4	$C_{43}H_{77}NO_8P$	766.5383	−12.0	−10.030
Phosphatidylserines (PS)				
PS 36:2	$C_{42}H_{77}NO_{10}P$	786.5284	−0.9	−8.830
PS 36:1	$C_{42}H_{79}NO_{10}P$	788.5443	−0.5	−7.352
PS 38:4	$C_{44}H_{77}NO_{10}P$	810.5272	−2.3	−10.043
PS 38:3	$C_{44}H_{79}NO_{10}P$	812.5430	−2.1	−6.212
PS 40:6	$C_{46}H_{77}NO_{10}P$	834.5261	−3.6	−6.371
PS 40:4	$C_{46}H_{81}NO_{10}P$	838.5593	−1.3	−7.859
Phosphatidylinositols				
PI 36:4	$C_{45}H_{78}O_{13}P$	857.5170	−1.9	−6.163
PI 38:5	$C_{47}H_{80}O_{13}P$	883.5321	−2.4	−4.348
PI 38:4	$C_{47}H_{82}O_{13}P$	885.5491	−0.9	−8.881

C. Compounds identified by SAM as relatively more abundant in ER compared to PR samples. Data were extracted from stromal regions.

Metabolites				
Hydroxybutyric acid	$C_4H_7O_3$	103.0404	−3.0	18.209
Hexose	$C_6H_{12}O_6Cl$	215.0327	−0.4	9.5241
Asp-His	$C_{10}H_{13}N_4O_5$	269.0883	1.8	5.1653
Uridine	$C_9H_{12}N_2O_6Cl$	279.0385	1.4	5.157
Monoacylglycerols				
MG 20:0	$C_{23}H_{46}O_4Cl$	421.3103	3.1	6.5347
Ceramides				
Cer d34:1	$C_{34}H_{67}NO_3Cl$	572.4797	3.1	10.64
Cer d42:2	$C_{42}H_{81}NO_3Cl$	682.5891	2.9	8.031
Cer d42:1	$C_{42}H_{83}NO_3Cl$	684.6081	2.1	8.0668

D. Compounds identified by SAM as relatively less abundant in ER compared to PR samples. Data were extracted from stromal regions.

Metabolites				
Succinic acid	$C_4H_5O_4$	117.0195	−1.4	−5.0948
Taurine	$C_2H_6NO_3S$	124.0078	0.7	−4.6595
Fatty Acids (FA)				
FA 9:1;O	$C_9H_{15}O_3$	171.1029	1.4	−5.5852
FA 11:1;O	$C_{11}H_{19}O_3$	199.1344	2.2	−4.4793
FA 16:1	$C_{16}H_{29}O_2$	253.2179	2.4	−6.796
FA 18:3	$C_{18}H_{29}O_2$	277.2165	2.9	−5.2488
FA 18:2	$C_{18}H_{31}O_2$	279.2336	2.3	−7.3715
FA 18:1	$C_{18}H_{32}O_2$	281.2493	2.5	−7.7215
FA 18:0	$C_{18}H_{35}O_2$	283.2648	1.9	−4.8951
FA 20:4	$C_{20}H_{31}O_2$	303.2333	1.1	−7.0052

Table 1 continued

D. Compounds identified by SAM as relatively less abundant in ER compared to PR samples. Data were extracted from stromal regions.				
FA 20:3	$C_{20}H_{33}O_2$	305.2476	3.3	−9.9855
FA 20:2	$C_{20}H_{35}O_2$	307.2638	−1.6	−9.4183
FA 20:1	$C_{20}H_{37}O_2$	309.2795	2.3	−9.1167
FA 22:6	$C_{22}H_{31}O_2$	327.2326	1.2	−5.0138
FA 22:5	$C_{22}H_{33}O_2$	329.2477	2.7	−5.781
FA 22:4	$C_{22}H_{35}O_2$	331.2649	2.0	−10.495
FA 22:3	$C_{22}H_{37}O_2$	333.2794	1.5	−7.3874
FA 22:2	$C_{22}H_{39}O_2$	335.2952	1.2	−5.069
FA 22:1	$C_{22}H_{41}O_2$	337.3117	1.5	−7.3867
FA 24:4	$C_{24}H_{39}O_2$	359.2947	2.5	−8.9018
FA 24:2	$C_{24}H_{43}O_2$	363.3262	1.9	−5.7095
FA 24:1	$C_{24}H_{45}O_2$	365.3427	0.5	−8.6896
FA 24:0	$C_{24}H_{47}O_2$	367.3586	1.2	−6.4545
Monoacylglycerols (MG)				
MG 16:0	$C_{19}H_{38}O_4Cl$	365.2458	1.6	−4.9891
Phosphatidic acids (PA)				
PA 35:2	$C_{38}H_{70}O_8P$	685.4814	0	−7.2447
PA 35:1	$C_{38}H_{72}O_8P$	687.497	0	−6.1941
PA 36:2	$C_{39}H_{72}O_8P$	699.4971	0.1	−7.4984
PA 36:1	$C_{39}H_{74}O_8P$	701.5126	0.1	−6.2007
PA 37:4	$C_{40}H_{70}O_8P$	709.4815	0.2	−7.8465
PA 37:3	$C_{40}H_{70}O_8P$	711.4971	0.1	−9.3891
PA 37:2	$C_{40}H_{74}O_8P$	713.5129	0.3	−8.9105
PA 38:3	$C_{41}H_{74}O_8P$	725.5126	−0.1	−7.6253
PA 38:2	$C_{41}H_{76}O_8P$	727.5278	−0.7	−7.9704
PA 39:5	$C_{42}H_{72}O_8P$	735.4974	0.5	−7.9133
PA 39:4	$C_{42}H_{74}O_8P$	737.5126	−0.1	−9.1543

NACT tissues compared to pre-chemotherapy ones (Table 3C, D). Small metabolites (but not lipids) with lower relative abundances in the epithelial regions of post-NACT ER tissues included glycerophosphoethanolamine, citrate, glutamic acid, hypoxanthine, aspartate, pyroglutamate, fumarate, and uracil. Conversely, hydroxyglutaric acid was the only small metabolite with a lower relative abundance in the epithelial areas of post-NACT PR tissues.

In the epithelial regions, fatty acid species had a lower relative abundance in post-NACT tissues for both ER and PR tumors, while the relative abundance of phosphatidic acids was higher in the epithelial areas of post-NACT tissues for both ER and PR tumors. Indeed, phosphatidic acids were detected at higher relative abundances after chemotherapy in both ER and PR tumors (Fig. 3a). Interestingly, ceramides were highly abundant in the epithelial areas of post-NACT ER tumors. In the stromal areas, glycerophosphoinositol species were highly abundant in post-NACT tissues in both ER and PR tumors, while glycerophosphoserine and glycerophosphoethanolamine species were particularly abundant in post-NACT PR tumors. Heatmaps show distinct distributions of the normalized ion intensities of lipid species with different abundances in the epithelial areas (Fig. 4a, b) and stromal areas (Fig. 4c, d) in both pre- and post-NACT tissues from ER and PR tumors.

To investigate if the metabolites that had higher or lower relative abundances in post- versus pre-NACT tissues of ER and PR tumors were related to specific metabolic pathways, we analyzed the non-lipid metabolites identified with DESI-MS. The histograms in Fig. 3c, d represent the higher and lower relative abundances of metabolites in ER and PR tumors of post- versus pre-NACT samples. The epithelial regions of post-NACT samples from ER tumors showed lower relative abundances of uracil, fumarate, pyroglutamate, aspartate, hypoxanthine, glutamic acid, citrate, and galactosylglycerol (Table 3A), which are involved in the "urea cycle," "phenylalanine and tyrosine metabolism," and "nucleotide metabolism" pathways (FDR-adjusted $p < 0.01$) (Supplementary Table 6A, B), whereas several metabolites, including hydroxy valeric acid, taurine, leucinic acid, hydroxyniconitic acid, and glutamine (Table 3B), which had higher relative abundances in the epithelial regions of ER tumors, are involved in the "TP53-regulated metabolic genes" and "metabolism of nucleotides" pathways (FDR-adjusted $p < 0.05$) (Supplementary Table 7A, B). Metabolites with lower abundances in the post-NACT stromal regions of ER tumors, including uracil, hypoxanthine, glutamic acid, xanthine, and inosine (Table 3E), were associated with the pathways "metabolism of nucleotides" (FDR-adjusted < 0.01), "nucleotide salvage" (FDR-adjusted $p < 0.01$), and "purine catabolism" (FDR-adjusted $p < 0.01$) (Supplementary Table 8A, B), while metabolites such as valeric acid, fumaric acid, taurine, glutarate semialdeyde, and succininc acid (Table 3F), which had high relative abundances in the stromal regions, were mostly involved in the "urea cycle" and "citric acid cycle" pathways (FDR-adjusted $p < 0.05$) (Supplementary Table 9A, B).

In the epithelial regions of post-NACT PR tumors, taurine, glutamine, xanthine, aconitic acid, ascorbic acid, hexose, asp-his, inosine, and glutathione (Table 3D) had higher relative abundances and were mostly associated with the "metabolism of nucleotides" and "TP53 regulated-metabolic genes" pathways

Table 2. Summary of deregulated pathways.

A. Metabolic pathways upregulated in pre-chemotherapy tissues from ER and PR tumors.

Upregulated pathways in chemo-naïve tissues of ER versus PR

ER		PR	
Stroma	Epithelium	Stroma	Epithelium
Pyrimidine salvage (entities ratio 0.01)	Respiratory electron transport[a] (entities ratio 0.008)	Transport of bile salts and organic acids metal ions and amine compounds[a] (entities ratio 0.04)	Recycle of bile acids and salts (entities ratio 0.01)
	Metabolism of amino acids and derivatives (entities ratio 0.15)	Oxygen-dependent proline hydroxylation of Hypoxia-inducible Factor Alpha[a] (entities ratio 0.003)	Pyrimidine salvage (entities ratio 0.01)
			Pyrimidine catabolism (entities ratio 0.02)

B. Metabolic pathways upregulated and downregulated in post- versus pre-chemotherapy tissues from ER and PR tumors.

Deregulated pathways in post-chemo versus pre-chemo tissues of ER and PR

ER		PR		
Stroma	Epithelium	Stroma	Epithelium	
Upregulated	Urea cycle (entities ratio 0.12)	TP53 Regulates Metabolic Genes (entities ratio 0.01)	Aspartate and asparagine metabolism (entities ratio 0.01)	TP53 Regulates Metabolic Gene (entities ratio 0.01)
	Citric acids cycle (entities ratio 0.02)	Metabolism of nucleotides (entities ratio 0.08)	Phenylalanine and tyrosine metabolism (entities ratio 0.02)	Metabolism of nucleotides (entities ratio 0.08)
			Nucleotide biosynthesis (entities ratio 0.03)	
			Urea cycle (entities ratio 0.01)	
Downregulated	Metabolism of nucleotides[b] (entities ratio 0.08)	Urea cycle[b] (entities ratio 0.01)	GABA degradation and synthesis (entities ratio 0.01)	2-Hydroxyglutarate
	Nucleotide salvage[b] (entities ratio 0.03)	Metabolism of nucleotides[b] (entities ratio 0.08)		
	Purine catabolism[b] (entities ratio 0.03)	Phenylalanine and tyrosine metabolism[b] (entities ratio 0.02)		

[a] $p < 0.05$ probability score corrected for false-discovery rate (FDR) using Benjamini-Hochberg method.
[b] $p < 0.01$ probability score corrected for false-discovery rate (FDR) using Benjamini-Hochberg method.

(FDR-adjusted $p < 0.05$) (Supplementary Table 10A, B, Table 2B). In the stromal regions of post-NACT PR tumors, the metabolites with higher abundances included fumaric acid, taurine, pyroglutamic acid, aspartic acid, and aconitic acid (Table 3G), which were related to the "aspartate and asparagine metabolism," "phenylalanine and tyrosine metabolism," and "nucleotide biosynthesis" and "urea cycle" pathways (Supplementary Table 11A, B, Table 2B), whereas less abundant metabolites, such as valeric acid, glutarate semialdehyde, succinic acid, hydroxyvaleric acid, malic acid, glutamic acid, and hydroxyglutaric acid, were associated with the "GABA degradation and synthesis" pathway (Supplementary Table 12A, B, Table 2B). Table 2B summarizes the deregulated pathways in post-NACT ER and PR tissues compared with pre-treatment tissues.

Sparse partial least squares discriminant analysis (sPLS-DA) of the data acquired from pre- and post-NACT samples in both ER and PR tumors showed a clear separation of the two tissue groups in the tri- or bi-dimensional score plots (Fig. 4e, f). These results indicate that different adaptive metabolic changes occur in tissues based on response to NACT.

Quantitative proteomic and phosphoproteomic analyses of pre-chemotherapy samples from ER and PR tumors

To identify differentially expressed enzymes and phosphoproteins in PR versus ER tumors, we generated global proteomic and phosphoproteomic data for whole-tumor equivalent collections of pre-chemotherapy samples, as described previously[13]. A total of 7148 proteins and more than 1075 phosphosites were co-quantified across cases (Supplemental Tables 13–19). We selected proteins and phosphosites with significantly different expressions based on clinical response and metabolic pathways previously identified by DESI-MS. Pathways with the highest number of proteins quantified included the "metabolism of amino acids and derivatives," "metabolism of nucleotides," and "respiratory electron transport and related" pathways. Differential analysis revealed that most proteins and phosphosites that differed significantly (LIMMA $p < 0.05$, ±1.5-fold change) between PR and ER cases mapped to the "metabolism of amino acids and derivatives" and "metabolism of nucleotides" pathways (z-score = 0.728 p-value 1.69E-13, derived from Ingenuity Pathway Analysis) (Fig. 5a). Principal component analysis of these proteins by case revealed a distinct separation of the pre-NACT PR and ER tumors (Fig. 5b).

The quantitative proteomic analysis confirmed that phosphosites, which are related to the metabolism of nucleotides and particular pyrimidines, were significantly elevated in the PR tumors, which was concordant with the DESI-MS data (Supplementary Tables 14, 16, and 18). Interestingly, uridine (which DESI-MS revealed to have a high relative abundance in the tumor epithelium of pre-NACT PR samples), which serves as a substrate for cytidine 5-prime triphosphate synthetase (CTPS1), was highly abundant in pre-NACT PR samples (logFC 0.97, LIMMA $p = 0.008$)

Table 3. Attribution of compounds for post- versus pre-chemotherapy tumors (the m/z data was acquired using DESI-MS imaging in the negative ion mode; attributions were assigned based on high mass accuracy and MS/MS measurements).

A. Compounds identified by SAM as relatively less abundant in post- compared to pre-chemotherapy samples. Data were extracted from epithelial regions of ER samples.

Tentative attribution	Molecular formula	Detected *m/z*	Mass error (ppm)	SAM score
Metabolites				
Uracil	$C_4H_3O_2N_2$	111.0199	−0.9	−20.440
Fumarate	$C_{47}H_{84}O_{13}P$	115.0039	1.7	−4.562
Pyroglutamate	$C_5H_6NO_3$	128.0355	1.6	−3.348
Aspartate	$C_4H_6NO_4$	132.0305	2.3	−4.681
Hypoxanthine	$C_5H_3ON_4$	135.0317	3.5	−22.383
Glutamic acid	$C_5H_8NO_4$	146.0449	−6.7	−5.777
Citrate	$C_6H_7O_7$	191.0193	−2.1	−4.788
Glycerophosphoethanolamine	$C_5H_{13}O_6NP$	214.0481	−2.3	−10.391
Galactosylglycerol or Glucosylglycerol	$C_9H_{17}O_8$	253.0931	0.8	−16.093
Fatty acids (FA)				
FA 9:0	$C_9H_{17}O_2$	157.1235	0.6	−10.222
FA 14:3	$C_{14}H_{21}O_2$	221.1547	0.0	−15.669
FA 14:1	$C_{14}H_{25}O_2$	225.1862	0.9	−9.174
FA 14:0	$C_{14}H_{27}O_2$	227.2014	−1.1	−7.506
FA 16:2	$C_{16}H_{27}O_2$	251.2008	3.6	−6.347
FA 16:1	$C_{16}H_{29}O_2$	253.2177	1.6	−8.238
FA 18:1	$C_{18}H_{32}O_2$	281.2492	2.1	−26.771
FA 18:0	$C_{18}H_{35}O_2$	283.2648	1.9	−13.642
FA 20:3	$C_{20}H_{33}O_2$	305.2483	−1.0	−11.617
FA 20:2	$C_{20}H_{35}O_2$	307.2638	−1.6	−29.185
FA 20:1	$C_{20}H_{37}O_2$	309.2795	−2.3	−31.634
FA 20:0	$C_{20}H_{39}O_2$	311.2952	−1.3	−9.691
FA 18:0	$C_{18}H_{36}O_2Cl$	319.2407	−0.6	−4.592
FA 22:4	$C_{22}H_{35}O_2$	331.2649	2.0	−24.749
FA 22:3	$C_{22}H_{37}O_2$	333.2794	−1.5	−17.342
FA 22:2	$C_{22}H_{39}O_2$	335.2952	−1.2	−19.512
FA 22:1	$C_{22}H_{41}O_2$	337.3102	−3.0	−32.050
FA 22:0	$C_{22}H_{43}O_2$	339.3269	−0.1	−17.807
FA 24:5	$C_{24}H_{37}O_2$	357.2807	2.2	−6.846
FA 24:4	$C_{24}H_{39}O_2$	359.2947	−2.5	−9.482
FA 24:3	$C_{24}H_{41}O_2$	361.3106	−1.7	−9.997
FA 24:2	$C_{24}H_{43}O_2$	363.3262	−1.9	−15.153
FA 24:1	$C_{24}H_{45}O_2$	365.3427	0.5	−32.048
FA 24:0	$C_{24}H_{47}O_2$	367.3586	1.2	−22.423
FA 26:5	$C_{26}H_{41}O_2$	385.3105	−1.8	−4.939
FA 26:2	$C_{26}H_{47}O_2$	391.3587	1.4	−7.404
FA 26:1	$C_{26}H_{49}O_5$	393.3734	−1.0	−15.907
FA 11:1;O	$C_{11}H_{19}O_3$	199.1344	2.2	−14.381
Diacylglycerols (DG)				
DG 34:2	$C_{37}H_{68}O_5Cl$	627.4758	−0.4	−7.127
DG 34:1	$C_{37}H_{70}O_5Cl$	629.4913	−0.6	−11.224
DG 36:3	$C_{39}H_{70}O_5Cl$	653.4928	1.6	−10.206
DG 36:2	$C_{39}H_{72}O_5Cl$	655.5080	1.0	−19.553
DG 38:4	$C_{41}H_{72}O_5Cl$	679.5089	2.2	−6.385
Ceramides (Cer)				
Cer d34:0	$C_{34}H_{69}NO_3Cl$	574.4962	−1.6	−9.628
Cer d38:1	$C_{38}H_{75}NO_3Cl$	628.5462	3.3	−6.822
Glycerophosphoethanolamines (PE)				
PE O-34:2 or PE P-34:1	$C_{39}H_{75}NO_7P$	700.5272	−2.1	−8.500
PE 34:2	$C_{39}H_{73}NO_8P$	714.5052	−3.8	−13.740

Table 3 continued

A. Compounds identified by SAM as relatively less abundant in post- compared to pre-chemotherapy samples. Data were extracted from epithelial regions of ER samples.

Tentative attribution	Molecular formula	Detected *m/z*	Mass error (ppm)	SAM score
PE 34:1	$C_{39}H_{75}NO_8P$	716.5248	1.7	−20.240
PE O-36:3 or P-36:2	$C_{41}H_{77}NO_7P$	726.5459	2.2	−12.602
PE O-36:2 or PE P-36:1	$C_{41}H_{79}NO_7P$	728.5631	4.3	−14.666
PE 36:3	$C_{41}H_{75}NO_8P$	740.5232	−0.5	−24.207
PE 36:2	$C_{41}H_{77}NO_8P$	742.5407	2.0	−23.970
PE 36:1	$C_{41}H_{79}NO_8P$	744.5533	−2.1	−12.773
PE O-38:6 or PE P-38:5	$C_{43}H_{75}NO_7P$	748.5255	−4.2	−8.770
PE O-38:5 or PE P-38:4	$C_{43}H_{77}NO_7P$	750.5443	0.0	−6.960
PE O-38:4 or PE P-38:3	$C_{43}H_{79}NO_7P$	752.5554	−6.1	−11.648
PE 38:5	$C_{43}H_{75}NO_8P$	764.5244	1.1	−15.555
PE 38:3	$C_{43}H_{79}NO_8P$	768.5546	−0.4	−15.319
PE 39:6	$C_{44}H_{75}NO_8P$	776.5258	2.9	−4.261
PE 40:5	$C_{45}H_{79}NO_8P$	792.5545	−1.6	−12.876
PE 37:1	$C_{42}H_{82}NO_8PCl$	794.5485	0.8	−8.316
PE O-40:8 or PE P-40:7	$C_{45}H_{76}NO_8PCl$	808.5068	1.8	−7.000
PE 39:2	$C_{44}H_{84}NO_8PCl$	820.5603	3.1	−6.123
PE 39:1	$C_{44}H_{86}NO_8PCl$	822.5730	−6.7	−6.590
Cardiolipins (CL)				
CL 70:7	$C_{79}H_{138}O_{17}P_2$	710.4697	−1.8	−10.258
CL 70:6	$C_{79}H_{140}O_{17}P_2$	711.4767	−3.0	−5.128
CL 72:8	$C_{81}H_{140}O_{17}P_2$	723.4766	−3.0	−9.789
CL 72:7	$C_{81}H_{142}O_{17}P_2$	724.4855	−1.6	−4.359
CL 72:6	$C_{81}H_{144}O_{17}P_2$	725.4940	−0.7	−9.349
CL 74:9	$C_{83}H_{142}O_{17}P_2$	736.4847	−2.7	−11.996
CL 74:8	$C_{83}H_{144}O_{17}P_2$	737.4921	−3.3	−10.454
CL 74:7	$C_{83}H_{146}O_{17}P_2$	738.5015	−1.1	−16.994
CL 74:6	$C_{83}H_{148}O_{17}P_2$	739.5074	−3.7	−5.309
Phosphatidic Acids (PA)				
PA 36:2	$C_{39}H_{72}O_8P$	699.4948	−3.1	−6.786
PA 36:1	$C_{39}H_{74}O_8P$	701.5120	−1.0	−5.129
Glycerophosphoinositols (PI)				
LysoPI 18:0	$C_{27}H_{52}O_{12}P$	599.3215	2.2	−7.078
PI 32:1	$C_{41}H_{76}O_{13}P$	807.5016	−1.6	−12.308
PI 34:2	$C_{43}H_{78}O_{13}P$	833.5166	−2.4	−21.550
PI 34:1	$C_{43}H_{80}O_{13}P$	835.5342	0.0	−32.764
PI 36:4	$C_{45}H_{78}O_{13}P$	857.5163	−2.7	−15.171
PI 36:3	$C_{45}H_{80}O_{13}P$	859.5347	0.6	−16.601
PI 36:2	$C_{45}H_{82}O_{13}P$	861.5486	−1.5	−33.085
PI 36:1	$C_{45}H_{84}O_{13}P$	863.5643	−1.4	−28.121
PI 38:5	$C_{47}H_{80}O_{13}P$	883.5332	−1.1	−17.153
PI 38:3	$C_{47}H_{84}O_{13}P$	887.5629	−2.9	−18.851
PI 38:2	$C_{47}H_{86}O_{13}P$	889.5752	−6.7	−20.727
PI 40:5	$C_{49}H_{84}O_{13}P$	911.5638	−1.9	−14.072
PI 40:4	$C_{49}H_{86}O_{13}P$	913.5793	−2.1	−19.153
Glycerophosphoglycerols (PG)				
LysoPG 18:1	$C_{24}H_{46}O_9P$	509.2881	−2.9	−8.881
PG 32:0	$C_{38}H_{75}O_{10}P$	721.5026	0.1	−14.381
PG 34:2	$C_{40}H_{74}O_{10}P$	745.5015	−1.5	−19.098
PG 36:2	$C_{42}H_{78}O_{10}P$	773.5358	2.6	−22.063
PG 36:1	$C_{42}H_{80}O_{10}P$	775.5507	1.6	−28.345
PG 38:5	$C_{44}H_{76}O_{10}P$	795.5153	−3.6	−8.290
PG 38:4	$C_{44}H_{78}O_{10}P$	797.5313	−3.1	−21.018

Table 3 continued

A. Compounds identified by SAM as relatively less abundant in post- compared to pre-chemotherapy samples. Data were extracted from epithelial regions of ER samples.

Tentative attribution	Molecular formula	Detected *m/z*	Mass error (ppm)	SAM score
PG 38:3	$C_{44}H_{80}O_{10}P$	799.5467	−3.5	−20.588
PG 40:7	$C_{46}H_{76}O_{10}P$	819.5160	−2.7	−9.366
PG 40:6	$C_{46}H_{78}O_{10}P$	821.5309	−3.5	−8.422
PG 40:5	$C_{46}H_{80}O_{10}P$	823.5496	0.2	−6.882
PG 38:1	$C_{44}H_{85}O_{10}PCl$	839.5527	−5.6	−22.818
PG 40:2	$C_{46}H_{87}O_{10}PCl$	865.5725	−0.7	−28.840
Glycerophosphoserines (PS)				
PS 35:2	$C_{41}H_{75}NO_{10}P$	772.5187	−6.8	−8.281
PS 36:2	$C_{42}H_{77}NO_{10}P$	786.5270	−2.7	−9.734
PS 37:1	$C_{43}H_{81}NO_{10}P$	802.5659	6.9	−3.325
PS 38:4	$C_{44}H_{77}NO_{10}P$	810.5296	0.7	−7.364
PS 38:3	$C_{44}H_{79}NO_{10}P$	812.5437	−1.2	−14.019
PS 38:2	$C_{44}H_{81}NO_{10}P$	814.5577	−3.3	−8.148
PS 38:1	$C_{44}H_{83}O_{10}NP$	816.5745	−1.8	−3.511
PS 39:4	$C_{45}H_{79}NO_{10}P$	824.5454	0.8	−7.984
PS 40:6	$C_{46}H_{77}NO_{10}P$	834.5271	−2.4	−15.284
PS 40:5	$C_{46}H_{79}NO_{10}P$	836.5406	−4.9	−27.667
PS 40:4	$C_{46}H_{81}NO_{10}P$	838.5644	4.8	−26.875
PS 40:3	$C_{46}H_{83}NO_{10}P$	840.5746	−1.7	−13.881
PS 40:1	$C_{46}H_{87}O_{10}NP$	844.6080	0.8	−6.663

B. Compounds identified by SAM as relatively more abundant in post- compared to pre-chemotherapy samples. Data were extracted from epithelial regions of ER samples.

Metabolites				
Hydroxyvaleric acid	$C_5H_9O_3$	117.0559	1.7	7.770
Taurine	$C_2H_6NO_3S$	124.0064	−8.0	21.448
Leucinic acid or Leucic acid	$C_6H_{11}O_3$	131.0721	1.6	5.152
Hydroxynicotinic acid	$C_6H_4NO_3$	138.0198	0.7	7.478
Glutamine	$C_5H_9N_2O_3$	145.0621	1.4	16.405
Xanthine	$C_5H_3O_2N_4$	151.0260	−0.7	8.581
Aconitic acid	$C_6H_5O_6$	173.0096	2.5	8.680
Ascorbic acid	$C_6H_7O_6$	175.0252	2.3	55.475
Hexose	$C_6H_{11}O_6$	179.0562	0.5	19.654
Methylaconitate	$C_7H_7O_6$	187.0252	2.1	13.749
Ribitol or Xylitol	$C_5H_{12}O_9Cl$	187.0363	−4.6	36.741
Galactonic or Gluconic acid	$C_6H_{11}O_7$	195.0511	0.1	5.483
Hexose	$C_6H_{12}O_6Cl$	215.0327	−0.4	28.667
Methyluric acid	$C_6H_6N_4O_3Cl$	217.0121	3.4	12.073
Inosine	$C_{10}H_{11}N_4O_5$	267.0735	0.0	21.397
Asp-His	$C_{10}H_{13}N_4O_5$	269.0883	−1.8	37.237
Glutathione	$C_{10}H_{16}N_3O_6S$	306.0773	2.5	36.893
Dehydrocholesterol	$C_{27}H_{44}OCl$	419.3021	−5.9	27.631
Fatty acids (FA)				
FA 15:0	$C_{15}H_{29}O_2$	241.2172	−0.4	15.165
FA 19:0	$C_{19}H_{37}O_2$	297.2792	−2.4	7.445
FA 20:5	$C_{20}H_{29}O_2$	301.2174	0.3	22.496
FA 20:4	$C_{20}H_{31}O_2$	303.2333	1.1	15.808
FA 22:6	$C_{22}H_{31}O_2$	327.2326	1.2	22.369
FA 20:4	$C_{20}H_{32}O_2Cl$	339.2088	2.4	25.097
FA 22:6	$C_{22}H_{32}O_2Cl$	363.2094	−0.6	17.398
FA 22:3	$C_{22}H_{38}O_2Cl$	369.2554	−2.7	12.146
FA 24:5	$C_{24}H_{38}O_2Cl$	393.2582	4.1	55.254

Table 3 continued

B. Compounds identified by SAM as relatively more abundant in post- compared to pre-chemotherapy samples. Data were extracted from epithelial regions of ER samples.				
FA 36:3	$C_{36}H_{63}O_4$	559.4735	0.6	7.954
Monoacylglycerols (MG) and Diacylglycerols (DG)				
MG 20:4	$C_{23}H_{38}O_4Cl$	413.2465	0.2	39.965
MG 20:3	$C_{23}H_{40}O_4Cl$	415.2631	2.5	12.391
MG 22:6	$C_{25}H_{38}O_4Cl$	437.2459	−1.1	17.631
DG 40:10	$C_{43}H_{63}O_5$	659.4680	−0.1	19.690
Ceramides (Cer)				
Cer d34:1	$C_{34}H_{67}NO_3Cl$	572.4818	0.5	13.771
Cer d38:2	$C_{38}H_{73}NO_3Cl$	626.5350	10.0	32.563
PI-Cer d27:2	$C_{33}H_{61}NO_{11}P$	678.3983	−0.7	20.687
Cer d42:1	$C_{42}H_{83}NO_3Cl$	684.6072	0.7	15.105
PE-Cer d36:1	$C_{38}H_{76}N_2O_6P$	687.5449	0.4	46.883
Cer d46:2	$C_{46}H_{89}NO_3Cl$	738.6601	8.7	21.894
Glycerophosphoethanolamines (PE)				
PE O-36:5 or PE P-36:4	$C_{41}H_{73}NO_7Cl$	722.5116	−1.9	17.341
PE 38:6	$C_{43}H_{73}NO_8P$	762.5082	0.4	14.431
PE O-38:3 or PE P-38:2	$C_{43}H_{82}NO_7PCl$	790.5535	1.5	18.181
PE 39:4	$C_{44}H_{80}NO_8PCl$	816.5310	−0.7	12.594
Cardiolipins (CL)				
CL 70:5	$C_{79}H_{142}O_{17}P_2$	712.4837	−4.2	20.813
CL 74:10	$C_{83}H_{140}O_{17}P_2$	735.4814	3.5	44.982
Phosphatidic Acids (PA)				
PA 24:2	$C_{37}H_{68}O_8P$	671.4676	2.8	25.761
PA 24:1	$C_{37}H_{70}O_8P$	673.4814	1.6	10.164
PA 35:2	$C_{38}H_{70}O_8P$	685.4819	0.8	19.362
PA 36:4	$C_{39}H_{68}O_8P$	695.4690	4.7	40.482
PA 36:3	$C_{39}H_{70}O_8P$	697.4815	0.2	11.986
PA 37:5	$C_{40}H_{68}O_8P$	707.4674	2.4	17.812
PA 37:2	$C_{40}H_{74}O_8P$	713.5129	0.3	22.091
PA 39:6	$C_{42}H_{70}O_8P$	733.4810	−0.5	27.702
PA 39:3	$C_{42}H_{76}O_8P$	739.5256	−3.7	14.616
PA 41:6	$C_{44}H_{74}O_8P$	761.5147	2.7	16.314
PA 41:5	$C_{44}H_{76}O_8P$	763.5256	−3.6	18.852
Glycerophosphoinositols (PI)				
LysoPI 15:0	$C_{24}H_{46}O_{12}P$	557.2729	−0.5	10.733
PI 32:0	$C_{41}H_{78}O_{13}P$	809.5158	−3.5	8.976
PI 38:6	$C_{47}H_{78}O_{13}P$	881.5196	1.1	9.944
PI 39:5	$C_{48}H_{83}O_{13}PCl$	933.5302	3.9	9.518
Glycerophosphoglycerols (PG)				
PG 40:8	$C_{46}H_{74}O_{10}P$	817.5011	1.7	8.858
PG 44:12	$C_{50}H_{74}O_{10}P$	865.4996	3.4	7.085
Glycerophosphoserines (PS)				
PS 36:1	$C_{42}H_{79}NO_{10}P$	788.5466	2.4	13.818
PS 41:6	$C_{46}H_{81}NO_{10}P$	848.5439	−0.9	7.492
PS 39:8	$C_{45}H_{72}NO_{10}PCl$	852.4524	−7.5	26.773
PS 42:1	$C_{48}H_{91}O_{10}NP$	872.6408	2.5	22.164
C. Compounds identified by SAM as relatively less abundant in post- compared to pre-chemotherapy samples. Data were extracted from epithelial regions of PR samples.				
Metabolites				
Hydroxyglutaric acid	$C_5H_7O_5$	147.0305	4.1	−7.003
Fatty acids (FA)				
FA 14:3	$C_{14}H_{21}O_2$	221.1550	1.3	−6.927

Table 3 continued

C. Compounds identified by SAM as relatively less abundant in post- compared to pre-chemotherapy samples. Data were extracted from epithelial regions of PR samples.

FA 14:1	$C_{14}H_{25}O_2$	225.1866	2.7	−6.208
FA 16:1	$C_{16}H_{29}O_2$	253.2179	2.4	−8.600
FA 17:1	$C_{17}H_{31}O_2$	267.2336	2.4	−12.007
FA 18:2	$C_{18}H_{31}O_2$	279.2336	2.3	−6.317
FA 18:1	$C_{18}H_{32}O_2$	281.2493	2.5	−17.734
FA 18:0	$C_{18}H_{35}O_2$	283.2648	1.9	−5.779
FA 19:1	$C_{19}H_{35}O_2$	295.2650	2.5	−9.818
FA 20:2	$C_{20}H_{35}O_2$	307.2638	−1.6	−18.639
FA 20:1	$C_{20}H_{37}O_2$	309.2795	2.3	−21.688
FA 20:0	$C_{20}H_{39}O_2$	311.2952	−1.3	−12.279
FA 22:4	$C_{22}H_{35}O_2$	331.2649	2.0	−13.417
FA 22:3	$C_{22}H_{37}O_2$	333.2794	−1.5	−8.500
FA 22:2	$C_{22}H_{39}O_2$	335.2952	−1.2	−13.027
FA 22:1	$C_{22}H_{41}O_2$	337.3117	1.5	−19.667
FA 23:0	$C_{23}H_{45}O_2$	353.3420	−1.4	−5.843
FA 24:4	$C_{24}H_{39}O_2$	359.2947	−2.5	−9.861
FA 24:3	$C_{24}H_{41}O_2$	361.3106	−1.7	−7.446
FA 24:2	$C_{24}H_{43}O_2$	363.3262	−1.9	−11.294
FA 24:1	$C_{24}H_{45}O_2$	365.3427	0.5	−18.486
FA 24:0	$C_{24}H_{47}O_2$	367.3586	1.2	−7.162
FA 26:2	$C_{26}H_{47}O_2$	391.3590	2.2	−12.245
FA 26:1	$C_{26}H_{49}O_5$	393.3734	−1.0	−11.849
Glycerophosphoethanolamines (PE)				
PE O-34:3 or PE P-34:2	$C_{39}H_{73}NO_7P$	698.5133	0.4	−8.520
PE O-34:2 or PE P-34:1	$C_{39}H_{75}NO_7P$	700.5272	−2.1	−7.230
PE 34:2	$C_{39}H_{73}NO_8P$	714.5052	−3.8	−7.365
PE 34:1	$C_{39}H_{75}NO_8P$	716.5248	1.7	−9.922
PE 35:3	$C_{40}H_{74}NO_8P$	726.5027	−7.2	−9.643
PE O-36:3 or PE P-36:2	$C_{41}H_{77}NO_7P$	726.5459	2.2	−8.766
PE 36:3	$C_{41}H_{75}NO_8P$	740.5232	−0.5	−9.819
PE 36:1	$C_{41}H_{79}NO_8P$	744.5533	−2.1	−7.509
Cardiolipins (CL)				
CL 70:7	$C_{79}H_{138}O_{17}P_2$	710.4697	−1.8	−7.162
CL 70:6	$C_{79}H_{140}O_{17}P_2$	711.4767	−3.0	−9.924
CL 70:4	$C_{79}H_{144}O_{17}P_2$	713.4935	−1.4	−9.373
CL 72:7	$C_{81}H_{142}O_{17}P_2$	724.4855	−1.6	−6.559
CL 72:6	$C_{81}H_{144}O_{17}P_2$	725.4940	−0.7	−11.899
CL 72:4	$C_{81}H_{148}O_{17}P_2$	727.5054	−2.0	−7.283
CL 74:8	$C_{83}H_{144}O_{17}P_2$	737.4921	−3.3	−5.934
CL 74:7	$C_{83}H_{146}O_{17}P_2$	738.5015	−1.1	−9.658
CL 74:6	$C_{83}H_{148}O_{17}P_2$	739.5074	−3.7	−6.328
Glycerophosphoinositols (PI)				
PI 34:1	$C_{43}H_{80}O_{13}P$	835.5342	0.0	−8.203
PI 36:2	$C_{45}H_{82}O_{13}P$	861.5486	−1.5	−9.421
PI 36:1	$C_{45}H_{84}O_{13}P$	863.5643	−1.4	−12.320
PI 40:4	$C_{49}H_{86}O_{13}P$	913.5811	−0.1	−8.275
Glycerophosphoglycerols (PG)				
PG 34:1	$C_{40}H_{76}O_{10}P$	747.5160	−2.9	−11.758
PG 36:3	$C_{42}H_{76}O_{10}P$	771.5152	−3.9	−9.188
PG 36:2	$C_{42}H_{78}O_{10}P$	773.5358	2.6	−7.498
PG 36:1	$C_{42}H_{80}O_{10}P$	775.5507	1.6	−6.307
PG 38:4	$C_{44}H_{78}O_{10}P$	797.5313	−3.1	−7.565
PG 38:3	$C_{44}H_{80}O_{10}P$	799.5467	−3.5	−7.821

Table 3 continued

C. Compounds identified by SAM as relatively less abundant in post- compared to pre-chemotherapy samples. Data were extracted from epithelial regions of PR samples.				
PG 38:2	$C_{44}H_{82}O_{10}P$	801.5639	−1.5	−6.257
PG 40:6	$C_{46}H_{78}O_{10}P$	821.5309	−3.5	−6.754
PG 40:5	$C_{46}H_{80}O_{10}P$	823.5496	0.2	−5.715
PG 38:1	$C_{44}H_{85}O_{10}PCl$	839.5527	−5.6	−6.945
PG 40:2	$C_{46}H_{87}O_{10}PCl$	865.5725	−0.7	−5.844
Glycerophosphoserines (PS)				
PS 36:2	$C_{42}H_{77}NO_{10}P$	786.5270	−2.7	−6.506
PS 40:6	$C_{46}H_{77}NO_{10}P$	834.5271	2.4	−6.066
PS 40:4	$C_{46}H_{81}NO_{10}P$	838.5644	−4.8	−8.518
PS 40:3	$C_{46}H_{83}NO_{10}P$	840.5746	−1.7	−8.019

D. Compounds identified by SAM as relatively more abundant in post- compared to pre-chemotherapy samples. Data were extracted from epithelial regions of PR samples.				
Metabolites				
Taurine	$C_2H_6NO_3S$	124.0064	−8.0	21.448
Glutamine	$C_5H_9N_2O_3$	145.0621	1.4	15.322
Xanthine	$C_5H_3O_2N_4$	151.0260	−0.7	12.537
Aconitic acid	$C_6H_5O_6$	173.0096	2.5	10.117
Ascorbic acid	$C_6H_7O_6$	175.0252	2.3	27.156
Hexose	$C_6H_{12}O_6Cl$	215.0327	−0.4	18.663
Asp-His	$C_{10}H_{13}N_4O_5$	269.0883	1.8	20.157
Inosine	$C_{10}H_{11}N_4O_5$	267.0735	0.0	11.295
Glutathione	$C_{10}H_{16}N_3O_6S$	306.0773	2.5	13.103
Fatty acids (FA)				
FA 16:0	$C_{16}H_{31}O_2$	255.2324	−2.4	9.961
FA 20:5	$C_{20}H_{29}O_2$	301.2174	0.3	12.822
FA 22:6	$C_{22}H_{31}O_2$	327.2326	−1.2	13.521
FA 20:4	$C_{20}H_{32}O_2Cl$	339.2088	−2.4	11.230
FA 24:6	$C_{24}H_{35}O_2$	355.2634	−2.5	9.375
FA 22:3	$C_{22}H_{38}O_2Cl$	369.2554	−2.7	14.855
FA 24:5	$C_{24}H_{38}O_2Cl$	393.2582	−4.1	12.955
Monoacylglycerols (MG) and Diacylglycerols (DG)				
MG 18:0	$C_{21}H_{40}O_4Cl$	391.2620	−0.2	10.376
MG 20:4	$C_{23}H_{38}O_4Cl$	413.2465	0.2	17.338
MG 20:3	$C_{23}H_{40}O_4Cl$	415.2631	2.5	20.052
MG 22:6	$C_{25}H_{38}O_4Cl$	437.2459	−1.1	15.148
DG 36:4	$C_{39}H_{68}O_5Cl$	651.4748	−2.0	9.042
DG 36:1	$C_{39}H_{74}O_5Cl$	657.5229	−0.2	9.097
Ceramides (Cer)				
Cer d46:2	$C_{46}H_{89}NO_3Cl$	738.6601	8.7	10.092
Glycerophosphoethanolamines (PE)				
PE O-38:3 or PE P38:2	$C_{43}H_{82}NO_7PCl$	790.5535	1.5	9.961
PE P-36:4 or PE O-36:5	$C_{41}H_{73}NO_7Cl$	722.5116	−1.9	11.627
PE 38:5	$C_{43}H_{75}NO_8P$	764.5244	1.1	10.616
PE 39:5	$C_{44}H_{77}NO_8P$	778.5378	−1.0	11.813
PE 40:5	$C_{45}H_{79}NO_8P$	792.5545	−1.6	−12.876
PE 39:4	$C_{44}H_{80}NO_8PCl$	816.5310	−0.7	11.928
PE 41:4	$C_{46}H_{84}NO_8PCl$	844.562	−1.4	9.197
Cardiolipins (CL)				
CL 74:10	$C_{83}H_{140}O_{17}P_2$	735.4814	3.5	10.836
CL 76:9	$C_{85}H_{146}O_{17}P_2$	750.5045	2.9	9.173
CL 80:8	$C_{89}H_{156}O_{17}P_2$	779.5440	3.3	9.578

Table 3 continued

D. Compounds identified by SAM as relatively more abundant in post- compared to pre-chemotherapy samples. Data were extracted from epithelial regions of PR samples.				
Phosphatidic acids (PA)				
LysoPA 19:0	$C_{22}H_{45}O_7P$	451.2859	7.0	10.894
PA 24:2	$C_{37}H_{68}O_8P$	671.4676	2.8	10.733
PA 36:4	$C_{39}H_{68}O_8P$	695.4690	4.7	13.224
PA 37:5	$C_{40}H_{68}O_8P$	707.4674	2.4	9.715
PA 37:2	$C_{40}H_{74}O_8P$	713.5129	0.3	9.836
PA 39:6	$C_{42}H_{70}O_8P$	733.4810	−0.5	12.086
Glycerophosphoinositols (PI)				
LysoPI 15:0	$C_{24}H_{46}O_{12}P$	557.2729	−0.5	10.667
LysoPI 32:0	$C_{41}H_{80}O_{12}P$	795.5396	0.4	9.086
PI O-33:2 or PI P-33:1	$C_{42}H_{79}O_{12}PCl$	841.5011	−1.0	9.257
PI P-35:2	$C_{44}H_{81}O_{12}PCl$	867.5158	−0.2	9.154
Glycerophosphoglycerols (PG)				
PG 40:8	$C_{46}H_{74}O_{10}P$	817.5011	−1.7	16.007
PG 44:12	$C_{50}H_{74}O_{10}P$	865.4996	−3.4	15.160
Glycerophosphoserines (PS)				
PS 36:1	$C_{42}H_{79}NO_{10}P$	788.5466	2.4	11.903
PS 39:8	$C_{45}H_{72}NO_{10}PCl$	852.4524	−7.5	17.193
E. Compounds identified by SAM as relatively less abundant in post- compared to pre-chemotherapy samples. Data were extracted from stromal regions of ER samples.				
Metabolites				
Uracil	$C_4H_3O_2N_2$	111.0199	−0.9	−11.953
Hypoxanthine	$C_5H_3ON_4$	135.0317	3.7	−22.577
Glutamic acid	$C_5H_8NO_4$	146.0449	−6.7	−10.498
Xanthine	$C_5H_3O_2N_4$	151.0260	−0.7	−17.540
Inosine	$C_{10}H_2N_4O_5$	267.0735	0.0	−16.967
Fatty acids (FA)				
FA 12:0	$C_{12}H_{23}O_2$	199.1699	−2.5	−5.449
FA 18:1	$C_{18}H_{32}O_2$	281.2478	−2.8	−8.885
FA 20:4	$C_{20}H_{31}O_2$	303.2333	1.1	−8.974
FA 20:2	$C_{20}H_{35}O_2$	307.2638	−1.6	−7.230
FA 20:1	$C_{20}H_{37}O_2$	309.2795	−2.3	−13.741
FA 20:0	$C_{20}H_{39}O_2$	311.2952	−1.3	−9.172
FA 18:1	$C_{18}H_{34}O_2Cl$	317.2245	−2.5	−8.859
FA 22:5	$C_{22}H_{33}O_2$	329.2477	−2.7	−6.274
FA 22:4	$C_{22}H_{35}O_2$	331.2649	2.0	−11.732
FA 22:3	$C_{22}H_{37}O_2$	333.2794	−1.5	−6.074
FA 22:1	$C_{22}H_{41}O_2$	337.3102	−3.0	−9.161
FA 20:4	$C_{20}H_{32}O_2Cl$	339.2088	−2.4	−20.489
FA 22:0	$C_{22}H_{43}O_2$	339.3269	0.0	−6.886
FA 24:5	$C_{24}H_{37}O_2$	357.2807	2.2	−3.911
FA 24:4	$C_{24}H_{39}O_2$	359.2947	−2.5	−7.490
FA 24:1	$C_{24}H_{45}O_2$	365.3427	0.5	−23.955
FA 24:0	$C_{24}H_{47}O_2$	367.3586	1.2	−19.080
FA 24:5	$C_{24}H_{38}O_2Cl$	393.2582	4.1	−9.357
FA 11:1;O	$C_{11}H_{19}O_3$	199.1337	−1.4	−5.492
Monoacylglycerols (MG) and Diacylglycerols (DG)				
MG 18:2	$C_{21}H_{38}O_4Cl$	389.2478	3.3	−9.341
MG 18:0	$C_{21}H_{40}O_4Cl$	391.2620	−0.2	−12.385
MG 20:0	$C_{23}H_{46}O_4Cl$	421.3103	3.1	−23.749
DG 34:2	$C_{37}H_{68}O_5Cl$	627.4758	−0.4	−5.296

Table 3 continued

E. Compounds identified by SAM as relatively less abundant in post- compared to pre-chemotherapy samples. Data were extracted from stromal regions of ER samples.				
DG 34:1	$C_{37}H_{70}O_5Cl$	629.4913	−0.6	−7.707
DG 36:3	$C_{39}H_{70}O_5Cl$	653.4928	1.6	−6.659
DG 36:2	$C_{39}H_{72}O_5Cl$	655.5080	1.0	−11.045
DG 38:4	$C_{41}H_{72}O_5Cl$	679.5089	2.2	−4.582
Ceramides (Cer)				
Cer d32:1	$C_{32}H_{63}NO_3Cl$	544.4519	0.9	−19.867
Cer d34:2	$C_{34}H_{65}NO_3Cl$	570.4655	−1.8	−19.259
Cer d34:0	$C_{34}H_{69}NO_3Cl$	574.4962	−1.6	−19.485
Cer d38:1	$C_{38}H_{75}NO_3Cl$	628.5462	3.3	−6.822
Cer d40:1	$C_{40}H_{79}NO_3Cl$	656.5752	−0.1	−18.481
PI-Cer d27:2	$C_{33}H_{61}NO_{11}P$	678.3983	−0.7	−4.402
Cer d40:1	$C_{42}H_{79}NO_3Cl$	680.5770	2.4	−11.772
PE-Cer d37:1	$C_{39}H_{79}N_2O_6PCl$	737.5359	−1.5	−14.636
Cer d46:2	$C_{46}H_{89}NO_3Cl$	738.6601	8.7	−13.640
Glycerophosphoethanolamines (PE)				
PE O-34:2 or PE P-34:1	$C_{39}H_{75}NO_7P$	700.5272	−2.1	−5.874
PE O-36:5 or PE P-36:4	$C_{41}H_{73}NO_7Cl$	722.5116	−1.9	−8.954
PE O-38:6 or PE P-38:5	$C_{43}H_{75}NO_7P$	748.5255	−4.2	−7.729
PE O-38:5 or PE P-36:4	$C_{43}H_{77}NO_7P$	750.5443	0.0	−11.090
PE O-38:3 or PE P-38:2	$C_{43}H_{82}NO_7PCl$	790.5535	1.5	−4.531
PE 37:1	$C_{42}H_{82}NO_8PCl$	794.5485	−0.8	−4.623
Cardiolipins (CL)				
CL 72:7	$C_{81}H_{142}O_{17}P_2$	724.4855	−1.6	−6.514
CL 72:6	$C_{81}H_{144}O_{17}P_2$	725.4940	0.7	−6.330
Glycerophosphoinositols (PI)				
PI 34:2	$C_{43}H_{78}O_{13}P$	833.5166	−2.4	−4.807
PI 34:1	$C_{43}H_{80}O_{13}P$	835.5342	0.0	−12.021
PI 36:4	$C_{45}H_{78}O_{13}P$	857.5163	−2.7	−6.558
PI 36:2	$C_{45}H_{82}O_{13}P$	861.5486	−1.5	−6.045
PI 36:1	$C_{45}H_{84}O_{13}P$	863.5643	−1.4	−14.574
PI 38:4	$C_{47}H_{82}O_{13}P$	885.5483	−1.8	−9.892
PI 38:3	$C_{47}H_{84}O_{13}P$	887.5629	−2.9	−9.073
PI 40:5	$C_{49}H_{84}O_{13}P$	911.5638	−1.9	−6.344
PI 40:4	$C_{49}H_{86}O_{13}P$	913.5793	−2.1	−7.552
Glycerophosphoglycerols (PG)				
PG 34:1	$C_{40}H_{76}O_{10}P$	747.5160	−2.9	−12.887
PG 36:1	$C_{42}H_{80}O_{10}P$	775.5507	1.6	−15.975
Glycerophosphoserines (PS)				
PS O-36:2 or PS P-36:1	$C_{42}H_{79}NO_9P$	772.5490	−1.0	−6.308
PS 38:4	$C_{44}H_{77}NO_{10}P$	810.5296	0.7	−9.858
PS 40:6	$C_{46}H_{77}NO_{10}P$	834.5271	−2.4	−14.218
PS 40:5	$C_{46}H_{79}NO_{10}P$	836.5406	−4.9	−16.751
PS 40:4	$C_{46}H_{81}NO_{10}P$	838.5644	4.8	−12.498
PS 42:6	$C_{48}H_{82}NO_{10}P$	862.5556	−5.5	−3.969

F. Compounds identified by SAM as relatively more abundant in post- compared to pre-chemotherapy samples. Data were extracted from stromal regions of ER samples.				
Metabolites				
Valeric acid	$C_5H_9O_2$	101.061	1.9	5.427
Fumaric acid	$C_4H_3O_4$	115.0035	−1.6	13.889
Taurine	$C_2H_6NO_3S$	124.0073	−0.7	13.426
Glutarate semialdehyde	$C_5H_7O_3$	115.0399	−1.5	5.951
Succinic acid	$C_4H_5O_4$	117.0195	1.4	8.33

Table 3 continued

F. Compounds identified by SAM as relatively more abundant in post- compared to pre-chemotherapy samples. Data were extracted from stromal regions of ER samples.				
Pyroglutamic acid	$C_5H_6NO_3$	128.0354	0.6	1.355
Aspartic acid	$C_4H_6NO_4$	132.0304	1.3	3.233
Malic acid	$C_4H_5O_5$	133.0141	−1.1	12.019
Hydroxyglutaric acid	$C_5H_7O_5$	147.0297	−1.3	15.204
Gluconic acid or Galactonic acid	$C_6H_{11}O_7$	195.051	0.0	8.924
Hexose	$C_6H_{12}O_6Cl$	215.0324	−1.8	25.277
Asp-His	$C_{10}H_{13}N_4O_5$	269.0883	−1.8	17.671
Fatty acids (FA)				
FA 9:0	$C_9H_{17}O_2$	157.1232	−1.3	9.331
FA 11:7	$C_{11}H_7O_2$	171.0454	1.2	10.622
FA 10:0	$C_{10}H_{19}O_2$	171.1387	−2.3	5.978
FA 11:0	$C_{11}H_{21}O_2$	185.1548	0.5	0.723
FA 13:3	$C_{13}H_{19}O_2$	207.1383	−3.9	2.271
FA 14:0	$C_{14}H_{27}O_2$	227.201	−3.1	3.873
FA 15:0	$C_{15}H_{29}O_2$	241.2167	−2.5	8.34
FA 16:1	$C_{16}H_{29}O_2$	253.2166	−2.8	2.816
FA 16:0	$C_{16}H_{31}O_2$	255.2322	−3.1	5.791
FA 17:1	$C_{17}H_{31}O_2$	267.2324	−2.2	3.69
FA 17:0	$C_{17}H_{33}O_2$	269.2478	−3.0	3.318
FA 16:0;O	$C_{16}H_{31}O_3$	271.2285	2.2	1.324
FA 18:3	$C_{18}H_{29}O_2$	277.2165	−2.9	7.989
FA 18:2	$C_{18}H_{31}O_2$	279.2322	−2.9	1.013
FA 18:0	$C_{18}H_{35}O_2$	283.2634	−3.2	2.611
FA 18:1;O	$C_{18}H_{33}O_3$	297.2428	−2.4	5.597
FA 20:5	$C_{20}H_{29}O_2$	301.2168	−1.7	4.08
Diacylglycerols (DG)				
DG 43:6	$C_{46}H_{78}O_5Cl$	745.5558	2.0	0.224
Glycerophosphoethanolamines (PE)				
PE 34:1	$C_{39}H_{75}NO_8P$	716.519	−6.4	1.184
PE 38:5	$C_{43}H_{75}NO_8P$	764.5216	−2.6	1.99
Phosphatidic acids (PA)				
PA 36:1	$C_{39}H_{74}O_8P$	701.5102	−3.5	6.809
PA 38:0	$C_{41}H_{81}O_8PCl$	767.5396	4.3	1.719
PA 43:7	$C_{46}H_{76}O_8P$	787.5278	−0.6	4.834
PA 45:7	$C_{48}H_{80}O_8P$	815.5575	−2.6	0.352
Glycerophosphoglycerols				
PG 34:2	$C_{40}H_{74}O_{10}P$	745.4978	−6.3	1.953
PG 36:4	$C_{42}H_{74}O_{10}P$	769.4995	−3.9	5.211
PG 38:4	$C_{44}H_{78}O_{10}P$	797.5315	−2.9	3.107
PG 40:8	$C_{46}H_{74}O_{10}P$	817.5	−3.1	7.942
PG 40:6	$C_{46}H_{78}O_{10}P$	821.5299	−4.7	5.911
PG 40:5	$C_{46}H_{81}O_{10}PCl$	859.5275	1.6	3.737
Glycerophosphoserines (PS)				
PS 34:1	$C_{40}H_{75}NO_{10}P$	760.5111	−3.02	8.04
PS 36:2	$C_{42}H_{77}NO_{10}P$	786.5262	−3.69	3.504
PS 40:2	$C_{46}H_{85}NO_{10}P$	842.5904	−1.54	2.065

G. Compounds identified by SAM as relatively more abundant in post- compared to pre-chemotherapy samples. Data were extracted from stromal regions of PR samples.				
Metabolites				
Fumaric acid	$C_4H_3O_4$	115.0035	−1.6	1.322
Taurine	$C_2H_6NO_3S$	124.0073	−0.7	21.157
Pyroglutamic acid	$C_5H_6NO_3$	128.0354	0.6	3.641

Table 3 continued

G. Compounds identified by SAM as relatively more abundant in post- compared to pre-chemotherapy samples. Data were extracted from stromal regions of PR samples.

Aspartic acid	$C_4H_6NO_4$	132.0304	1.3	7.146
Aconitic acid	$C_6H_5O_6$	173.0091	−0.4	3.392
Gluconic acid or Galactonic acid	$C_6H_{11}O_7$	195.051	−5.3	12.54
Hexose	$C_6H_{12}O_6Cl$	215.0324	−1.8	19.122
Asp-His	$C_{10}H_{13}N_4O_5$	269.0883	−1.8	20.157
Uridine	$C_9H_{12}N_2O_6Cl$	279.0385	−1.4	1.824
Fatty acids (FA)				
FA 9:0	$C_9H_{17}O_2$	157.1235	0.6	12.071
FA 10:0	$C_{10}H_{19}O_2$	171.1387	−2.3	11.921
FA 11:0	$C_{11}H_{21}O_2$	185.1548	0.5	2.680
FA 9:2	$C_9H_{14}O_2Cl$	189.0684	−2.1	1.391
FA 12:2	$C_{12}H_{19}O_2$	195.1387	−2.1	1.59
FA 13:3	$C_{13}H_{19}O_2$	207.1383	−3.9	3.376
FA(14:0)	C14H27O2	227.201	−3.1	7.26
FA 15:4	$C_{15}H_{21}O_2$	233.1547	0.0	2.254
FA 14:4;O	$C_{14}H_{19}O_3$	235.1338	−0.9	2.254
FA 15:0	$C_{20}H_{37}O_2$	241.2167	−2.3	5.397
FA 16:0	$C_{20}H_{39}O_2$	255.2322	−1.3	9.617
FA 19:0	$C_{19}H_{37}O_2$	297.2792	−2.4	0.853
FA 20:0	$C_{20}H_{39}O_2$	311.2948	−2.6	FA 20:0
FA 24:4	$C_{24}H_{39}O_2$	359.2945	−3.1	1.802
Ceramides (Cer)				
Cer d34:1	$C_{34}H_{67}NO_3Cl$	572.4797	−3.1	5.171
Cer d42:2	$C_{42}H_{81}NO_3Cl$	682.5891	−2.9	4.551
Glycerophosphoethanolamines (PE)				
PE 34:2	$C_{39}H_{73}NO_8P$	714.5125	6.4	3.216
PE O-36:5 or PE P-36:4	$C_{41}H_{73}NO_7P$	722.5104	−3.6	11.536
PE 36:2	$C_{41}H_{77}NO_8P$	742.5368	−3.2	2.06
PE 36:1	$C_{41}H_{79}NO_8P$	744.5519	−4.0	4.241
PE 37:5	$C_{42}H_{73}NO_8P$	750.5069	−1.3	5.344
PE 37:4	$C_{42}H_{75}NO_8P$	752.5268	4.3	5.244
PE 38:5	$C_{43}H_{75}NO_8P$	764.5216	−2.6	2.862
PE 38:4	$C_{43}H_{77}NO_8P$	766.5366	−3.4	0.425
PE 39:5	$C_{44}H_{77}NO_8P$	778.5363	−3.7	0.689
Cardiolipins (CL)				
CL 72:8	$C_{81}H_{141}O_{17}P_2$	723.4766	3.0	13.016
CL 72:7	$C_{81}H_{142}O_{17}P_2$	724.4855	1.6	6.596
Phosphatidic acids (PA)				
PA 34:1	$C_{37}H_{70}O_8P$	673.4776	−5.6	0.232
PA 36:2	$C_{39}H_{72}O_8P$	699.4942	−4.0	7.63
PA 36:1	$C_{39}H_{74}O_8P$	701.5102	−3.6	6.263
PA 35:0	$C_{38}H_{75}O_8PCl$	725.4895	0.1	1.202
PA 38:3	$C_{41}H_{74}O_8P$	725.5129	0.3	6.552
PA 41:6	$C_{44}H_{74}O_8P$	761.5141	1.8	2.944
PA 38:0	$C_{41}H_{81}O_8PCl$	767.5396	4.3	2.237
PA 43:7	$C_{46}H_{76}O_8P$	787.5278	−0.6	13.418
PA 43:6	$C_{46}H_{78}O_8P$	789.5452	1.5	14.853
PA 45:7	$C_{48}H_{80}O_8P$	815.5575	−2.6	7.342
PA 45:6	$C_{48}H_{82}O_8P$	817.5785	3.9	6.619
Glycerophosphoinositols (PI)				
PI 34:1	$C_{43}H_{80}O_{13}P$	835.5303	−4.7	1.149
PI 36:4	$C_{45}H_{78}O_{13}P$	857.5155	−3.6	10.541
PI 36:2	$C_{45}H_{82}O_{13}P$	861.5486	−1.5	0.449

Table 3 continued

G. Compounds identified by SAM as relatively more abundant in post- compared to pre-chemotherapy samples. Data were extracted from stromal regions of PR samples.				
PI 38:5	$C_{47}H_{80}O_{13}P$	883.5314	−3.2	7.812
PI 38:4	$C_{47}H_{82}O_{13}P$	885.5465	−3.8	2.522
Glycerophosphoglycerols (PG)				
PG 34:2	$C_{40}H_{74}O_{10}P$	745.4978	−6.3	10.578
PG 34:1	$C_{40}H_{76}O_{10}P$	747.5155	−3.6	9.167
PG 36:4	$C_{42}H_{74}O_{10}P$	769.4995	−3.9	11.536
PG 36:3	$C_{42}H_{76}O_{10}P$	771.5142	−5.2	9.769
PG 36:2	$C_{42}H_{78}O_{10}P$	773.5301	−4.8	17.46
PG 38:6	$C_{44}H_{74}O_{10}P$	793.5004	−2.6	1.432
PG 38:4	$C_{44}H_{78}O_{10}P$	797.5315	−2.9	5.684
PG 40:8	$C_{46}H_{74}O_{10}P$	817.5	−3.1	0.755
PG 40:6	$C_{46}H_{78}O_{10}P$	821.5299	−4.7	6.352
PG 40:5	$C_{46}H_{81}O_{10}PCl$	859.5275	1.6	9.626
PG 42:5	$C_{48}H_{85}O_{10}PCl$	887.5562	−1.4	0.826
Glycerophosphoserines (PS)				
PS 34:1	$C_{40}H_{75}NO_{10}P$	760.5111	−3.0	15.483
PS 35:3	$C_{41}H_{73}NO_{10}P$	770.5023	5.8	8.446
PS O-36:2 or PS P-36:1	$C_{42}H_{79}NO_9P$	772.5479	−2.5	5.33
PS 36:2	$C_{42}H_{77}NO_{10}P$	786.5262	−3.7	10.854
PS 36:1	$C_{42}H_{79}NO_{10}P$	788.5419	−3.6	21.855
PS O-38:5 or PS P-38:4	$C_{44}H_{77}NO_9P$	794.5341	−0.1	2.789
PS 37:4	$C_{43}H_{75}NO_{10}P$	796.5157	2.9	2.768
PS 38:3	$C_{44}H_{79}NO_{10}P$	812.5409	−4.7	9.888
PS 38:1	$C_{44}H_{83}NO_{10}P$	816.5726	−4.2	4.956
PS 40:2	$C_{46}H_{85}NO_{10}P$	842.5904	−1.5	8.10

H. Compounds identified by SAM as relatively less abundant in post- compared to pre-chemotherapy samples. Data were extracted from stromal regions of PR samples.				
Metabolites				
Valeric acid	$C_5H_9O_2$	101.061	1.9	−2.427
Glutarate semialdehyde	$C_5H_7O_3$	115.0399	−1.5	−4.447
Succinic acid	$C_4H_5O_4$	117.0195	1.4	−12.384
Hydroxyvaleric acid	$C_5H_9O_3$	117.0559	1.7	−7.855
Malic acid	$C_4H_5O_5$	133.0141	−1.1	−8.58
Glutamic acid	$C_5H_8NO_4$	146.0457	−1.2	−4.628
Hydroxyglutaric acid	$C_5H_7O_5$	147.0297	−1.3	−12.647
Fatty acids (FA)				
FA 9:1; O	$C_9H_{15}O_4$	171.1023	−1.8	−20.144
FA 11:1;O	$C_{11}H_{19}O_3$	199.1337	−1.4	−13.216
FA 12:0	$C_{12}H_{22}O_2$	199.1699	−2.3	−10.301
FA 16:1	$C_{16}H_{29}O_2$	253.2166	−2.8	−12.592
FA 17:1	$C_{17}H_{31}O_2$	267.2324	−2.2	−8.513
FA 16:0;O	$C_{16}H_{31}O_3$	271.2285	2.2	−8.934
FA 18:3	$C_{18}H_{29}O_2$	277.2165	−2.9	−7.175
FA 18:2	$C_{18}H_{31}O_2$	279.2322	−2.9	−13.189
FA 18:1	$C_{18}H_{33}O_2$	281.2478	−2.8	−11.404
FA 18:0	$C_{18}H_{35}O_2$	283.2634	−3.2	−3.155
FA 20:5	$C_{20}H_{29}O_2$	301.2168	−1.7	−12.692
FA 20:4	$C_{20}H_{31}O_2$	303.232	−3.3	−5.464
FA 20:3	$C_{20}H_{33}O_2$	305.2476	−3.3	−22.548
FA 20:2	$C_{20}H_{35}O_2$	307.2633	−3.3	−20.444
FA 20:1	$C_{20}H_{37}O_2$	309.2789	−3.2	−15.464
FA 22:6	$C_{22}H_{31}O_2$	327.2321	−2.8	−9.732

Table 3 continued

H. Compounds identified by SAM as relatively less abundant in post- compared to pre-chemotherapy samples. Data were extracted from stromal regions of PR samples.

FA 22:5	$C_{22}H_{33}O_2$	329.2477	−2.7	−9.96
FA 22:4	$C_{22}H_{35}O_2$	331.2632	−3.3	−19.011
FA 22:3	$C_{22}H_{37}O_2$	333.2787	−3.6	−16.218
FA 22:1	$C_{22}H_{41}O_2$	337.3104	−2.4	−16.04
FA 20:4	$C_{20}H_{32}O_2Cl$	339.2086	−2.9	−3.325
FA 22:0	$C_{22}H_{43}O_2$	339.3267	−0.6	−12.848
FA 24:5	$C_{24}H_{37}O_2$	357.2785	−3.9	−6.204
FA 24:2	$C_{24}H_{43}O_2$	363.3257	−3.3	−17.31
FA 24:1	$C_{24}H_{45}O_2$	365.3417	−2.2	−23.635
FA 24:0	$C_{24}H_{47}O_2$	367.3574	−2.2	−22.636
FA 24:6	$C_{24}H_{36}O_2Cl$	391.2439	7.7	−2.463
FA 26:2	$C_{26}H_{47}O_2$	391.3564	−4.6	−12.891
FA 24:5	$C_{24}H_{38}O_2Cl$	393.261	11.2	−4.285
FA 26:1	$C_{26}H_{49}O_2$	393.3721	−4.3	−15.643
FA 26:0	$C_{26}H_{51}O_2$	395.3881	−3.5	−10.224
Monoacylglycerols (MG) and Diacylglycerols (DG)				
MG 16:0	$C_{19}H_{38}O_4Cl$	365.2458	−1.6	−18.923
MG 18:0	$C_{21}H_{40}O_4Cl$	391.2620	−0.2	−12.385
MG 20:0	$C_{23}H_{46}O_4Cl$	421.3103	3.1	−23.749
MG 29:0	$C_{32}H_{63}O_4$	511.47	−6.3	−3.033
DG P-31:1	$C_{34}H_{63}O_4$	535.4717	−2.8	−11.621
DG O-31:1 or DG P-31:0	$C_{34}H_{65}O_4$	537.4878	−1.9	−14.271
DG P-33:2	$C_{36}H_{65}O_4$	561.4877	−2.0	−14.806
DG O-33:2 or DG P-33:1	$C_{36}H_{67}O_4$	563.5018	−4.8	−7.763
DG O-33:1 or DG P-33:0	$C_{36}H_{69}O_4$	565.5182	−3.4	−16.294
Glycerophosphoethanolamines (PE)				
PE 39:6	$C_{44}H_{75}NO_8P$	776.5211	−3.2	−3.52
PE O-42:6 or PE P-42:5	$C_{47}H_{84}NO_7PCl$	840.5686	0.7	−4.849
Phosphatidic acids (PA)				
PA 37:1	$C_{40}H_{76}O_8P$	715.5262	−2.9	−2.123
PA 38:2	$C_{41}H_{76}O_8P$	727.526	−3.2	−14.876
Glycerophosphoinositols (PI)				
PI 40:4	$C_{49}H_{86}O_{13}P$	913.5793	−2.1	−7.552
PI 39:5	$C_{48}H_{83}O_{13}PCl$	933.5323	6.2	−2.112
Glycerophosphoserines (PS)				
PS 38:4	$C_{44}H_{77}NO_{10}P$	810.5291	−1.0	−2.127
PS 40:6	$C_{46}H_{77}NO_{10}P$	834.5291	0.1	−12.505
PS 40:4	$C_{46}H_{81}NO_{10}P$	838.5604	0.7	−12.192

(Supplementary Table 18). CTPS1 catalyzes the conversion of uridine triphosphate into cytidine triphosphate and regulates intracellular rates of RNA, DNA, and phospholipid synthesis[14,15]; its phosphorylation is inhibitory, which could explain the higher abundance of uridine. Lastly, the increase of ornithine aminotransferase in PR tumors, measured by proteomic analysis, correlated well with the high relative abundances of molecules detected by DESI-MS that are associated with aspartate and asparagine pathways in the stroma (e.g., fumaric acid, taurine, aspartic acid, and glucose)[16].

For the four enzymes that were upregulated in the pre-NACT PR samples (Supplementary Tables 13, 15, and 17), we analyzed the correlation between mRNA expression and progression-free survival (PFS) in patients with HGSC from publicly available databases (Supplementary Fig. 2). Interestingly, higher expression of glycine decarboxylase (GLDC) was positively correlated with worse prognosis (HR 1.16, CI 1.00–1.35, $p = 0.046$) (KMplotter.com). We also investigated the expression of GLDC mRNA in several organs (gTEX.org) and the expression of its protein (Protein Atlas) and mRNA (TCGA) in several cancer types (Supplementary Fig. 3). GLDC mRNA expression is low in normal ovarian and fallopian tube samples, but it is detected at high protein levels in ovarian cancer. A possible mechanism explaining the metabolic interaction between stroma and cancer cells involving GLDC activity is proposed in Fig. 5c. We further explored the possible impact of GLDC expression on the response of ovarian cancer cells to chemotherapy. After consulting the public database DepMap Public 22Q4 at Cancer Cell Line Encyclopedia (CCLE), we identified the ovarian cancer cell lines with higher GLDC expression based on average [log2(TPM + 1)] expression (Supplementary Fig. 4A).

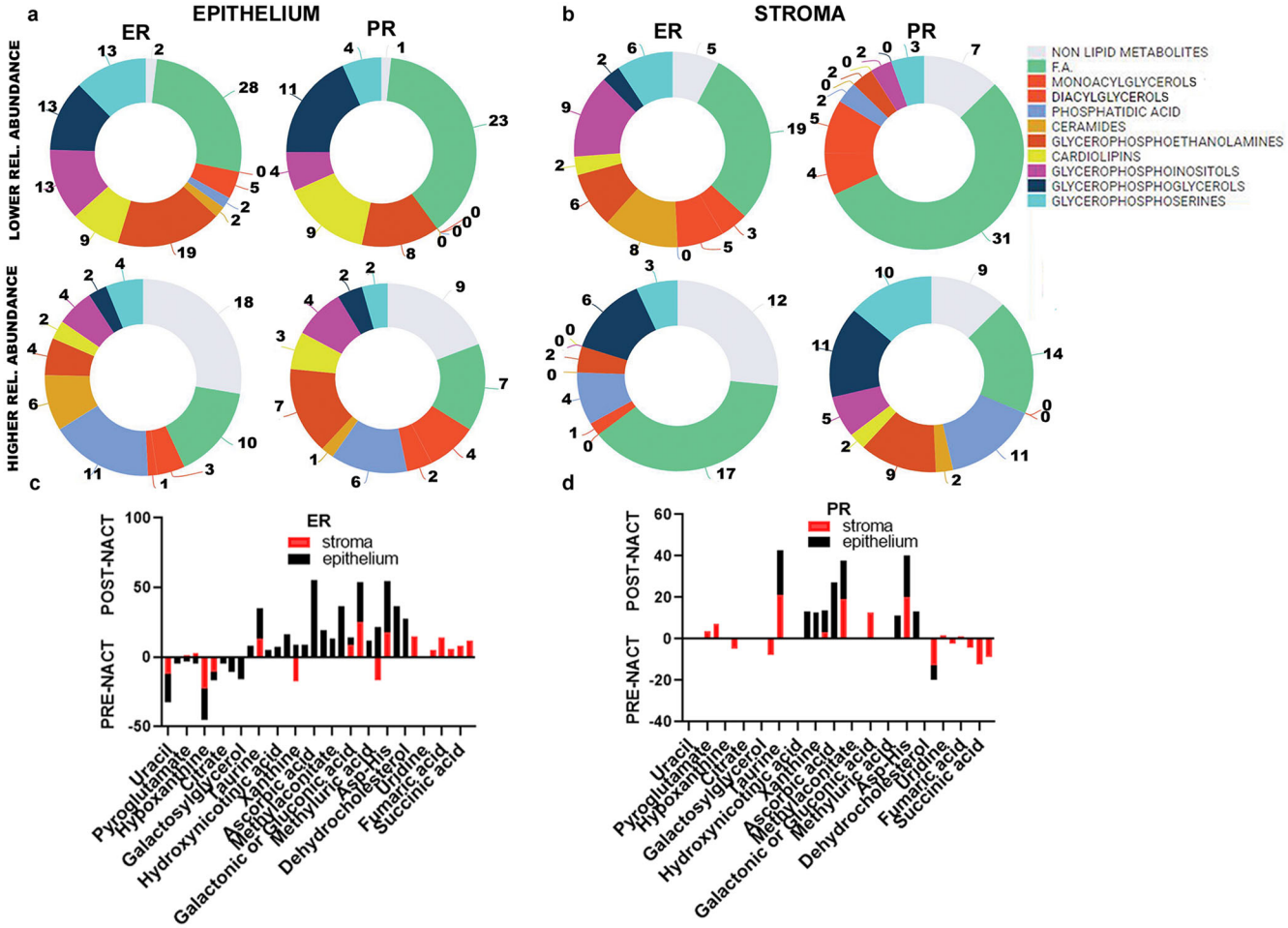

Fig. 3 Comparative analysis of high-grade serous ovarian cancer (HGSC) samples obtained post neoadjuvant chemotherapy (NACT) versus samples obtained prior neoadjuvant chemotherapy (NACT), based on excellent (ER) or poor (PR) response: lipids and small metabolites. a, **b** Pie charts summarize the number of lipids in each lipid class, with higher and lower relative abundance in the epithelium (**a**) and stroma (**b**) of ER and PR post- versus pre-chemotherapy tissues identified using DESI-MS analysis. **c**, **d** Histograms representing the relative abundances of small metabolites in the epithelium and stroma of ER (**c**) and PR (**d**) tumors of post- versus pre-NACT tissues identified using DESI-MS. The data shown in the pie charts were obtained from DESI-MS analysis of tumor tissue sections from pre-chemotherapy samples from 52 patients (30 ER and 22 PR) and post-chemotherapy samples from 37 patients (20 ER and 17 PR). ER excellent responders, PR poor responders.

IGROV1 cells are among the top two ovarian cancer cell lines listed in CCLE with the highest GLDC expression. We then measured GLDC mRNA expression in IGROV1 and other ovarian cancer cell lines and in the HIO 180 non-transformed epithelial ovarian cancer cells to confirm that IGROV1 had the highest GLDC expression among them (Supplementary Fig. 4B). Next, the level of GLDC mRNA in IGROV1 was evaluated after transient transfection with three silencing RNAs (siRNA29, siRNA35, siRNA03). SiRNA35 resulted in the lowest mRNA levels of GLDC (Supplementary Fig. 4C). Cell viability was then evaluated in IGROV1 cells transfected with siRNA35 or siRNA control and treated for 72 h with carboplatin. The IC50 level of carboplatin in IGROV1 cells transfected with siRNA35 was 3.3 times lower than the IC50 in IGROV1 cells transfected with siRNA control, 3.7 μM versus 12.3 μM ($P = 0.0003$, hypothesis test, alpha 0.05) (Supplementary Fig. 4D).

DISCUSSION

Relapse represents a major challenge in the treatment of patients with ovarian cancer, and studying the molecular changes related to therapy response is essential to identifying novel actionable targets. Nutrient availability inside the TME and paracrine communication influence the metabolic reprogramming of cancer cells, generating a complex metabolic profile[17]. In particular, reprogramming of nucleotide metabolism towards increased levels of nucleotide precursors and nucleotides has been found in recurrent tumor cells, including several cancer models[14,18]. Also, the metabolic dependency of ovarian cancer cells on neighboring stroma cells plays an important role in fueling tumor cell growth[15]. Many studies have investigated the metabolic interactions between the TME and cancer cells in inducing a permissive environment for tumor growth. The increased use of glucose and glutamine by cancer cells results in lactate accumulation, which decreases the activation of dendritic and T cells while stimulating the polarization of macrophages towards an M2-like phenotype[16,19]. Moreover, lactate stimulates angiogenesis[20] and promotes acidification of the TME. This stimulates the proteolytic activity of metalloproteinases[21], which in turn enhances extracellular matrix degradation and tumor invasion. Therefore, while much is known about how the metabolic interactions between stroma and cancer cells induce tumor cell proliferation and invasion, less is known about how these interactions promote resistance to chemotherapy. A few recent studies identified some important metabolic vulnerabilities in ovarian cancers that can be

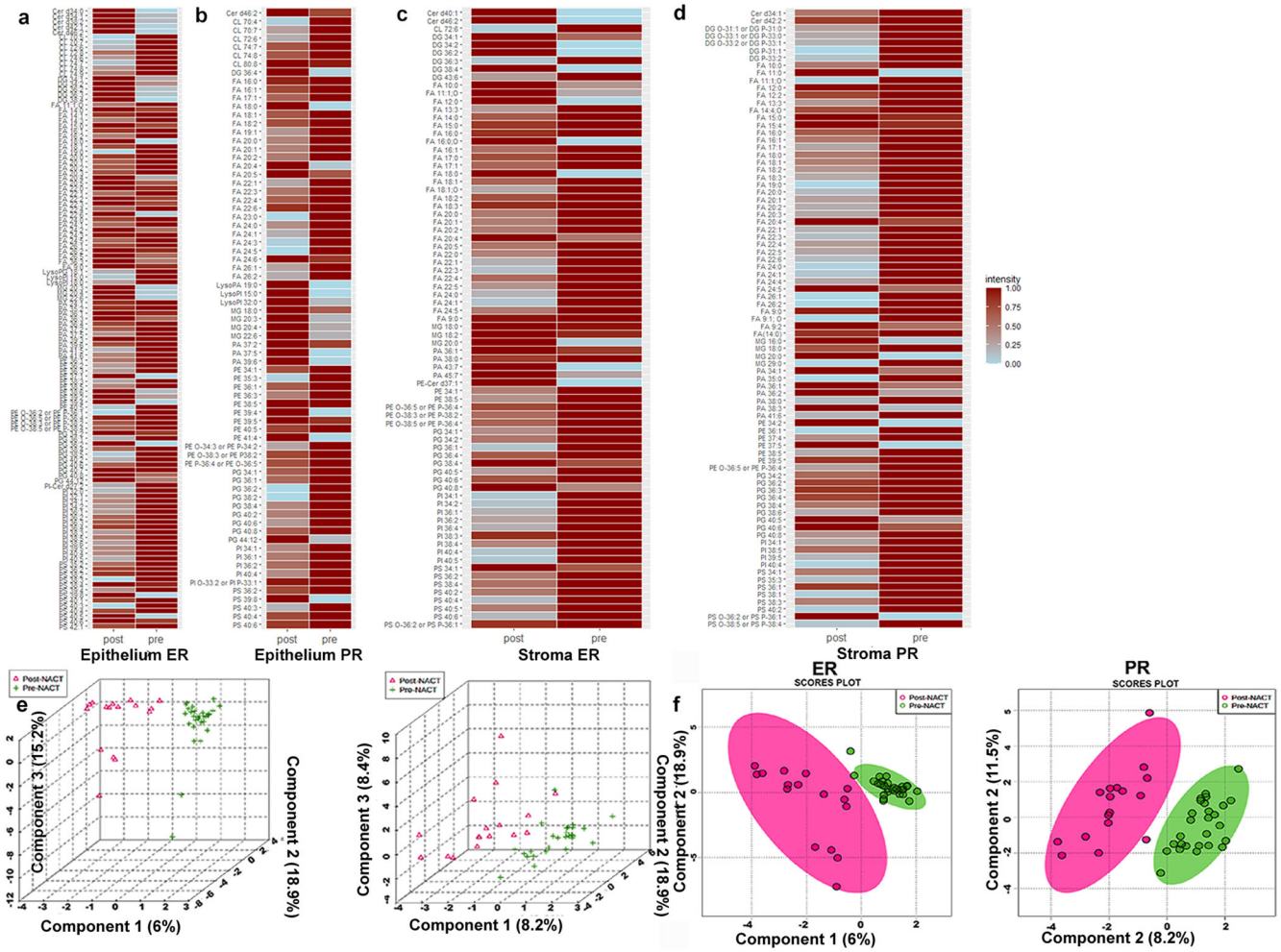

Fig. 4 Comparative analysis of high-grade serous ovarian cancer (HGSC) samples obtained post neoadjuvant chemotherapy (NACT) versus samples obtained prior neoadjuvant chemotherapy (NACT), based on excellent (ER) or poor (PR) response: lipids heatmaps and sPLS-DA plots. a, **b** Heatmaps representing the relative abundances of lipids in the epithelial areas of ER tumors (**a**); epithelial areas of PR tumors (**b**); stromal areas of ER tumors (**c**); and stromal areas of PR tumors (**d**). **e**, **f** Plots for sparse partial least squares discriminant analysis (sPLS-DA) in tri-dimensional (**e**) and bi-dimensional (**f**) settings. post post-NACT; pre pre-NACT; ER excellent responders, PR poor responders. For heatmap abbreviations see Tables 1 and 3. The data shown in the heatmaps were obtained from DESI-MS analysis of tumor tissue sections from pre-chemotherapy samples from 52 patients (30 ER and 22 PR) and post-chemotherapy samples from 37 patients (20 ER and 17 PR).

exploited to increase treatment response; these vulnerabilities include glutamine and serine metabolism[22,23]. To thoroughly study the metabolic heterogeneity of the HGSC TME in relation to therapy response, we performed a comparative analysis of metabolic species (nucleotides, proteins, sugars, and lipids) present in pre- and post-NACT tissues. We used DESI-MS imaging to obtain spatially resolved metabolomic information about the epithelial and stromal regions, and we used global proteomics and phosphoproteomics to corroborate the metabolic findings.

The use of highly clinically annotated samples, as presented here, is important for obtaining reliable results. When comparing the relative abundances of metabolites detected within the stromal regions of post- versus pre-NACT tissues, we found that PR tumors had higher abundances of fumaric acid, taurine, and aspartic acid, which are related to aspartate and asparagine metabolism. Interestingly, proliferating cells with impending glutamine depletion often adapt by utilizing asparagine, which is structurally similar to glutamine and can be used to fuel the TCA cycle, as an energy source[24,25]. It is plausible that an elevated demand for glutathione to counteract chemotherapy-induced cell damage may result in the depletion of glutamine in proliferating cells; in this scenario, stromal cells may support cancer cells by fueling them with asparagine to sustain their proliferation in tissues that respond less to chemotherapy. Moreover, the stroma of post-chemotherapy PR tissues showed elevated abundances of glycerophosphoserines (PS 36:1, PS 34:1, PS 36:2), which might be substrates for serine synthesis[26]. We believe that the increased nucleotide metabolism in PR cancer cells might be sustained by an increased influx of glycine and serine from the tumor stroma, leading to the increased activity of GLDC. GLDC fuels one-carbon metabolism via glycine breakdown to form CO_2, NH_3, and 5,10-methylene-tetrahydrofolate (CH2-THF)[27]; in particular, CH2-THF has been shown to be crucial for nucleotide synthesis[28,29]. As shown in other cancer types, GLDC may sustain nucleotide synthesis during cell proliferation in HGSC tumorigenesis[30,31]. However, an increase in nucleotide synthesis does not necessarily translate into a higher sensitivity to carboplatin-based chemotherapy (the main type of neoadjuvant chemotherapy used for ovarian cancer in our cohort and in general), since carboplatin does not show cell-cycle specificity[32].

Our findings suggest several strategies to overcome chemotherapy resistance in HGSC, including targeting glycerophosphoserine

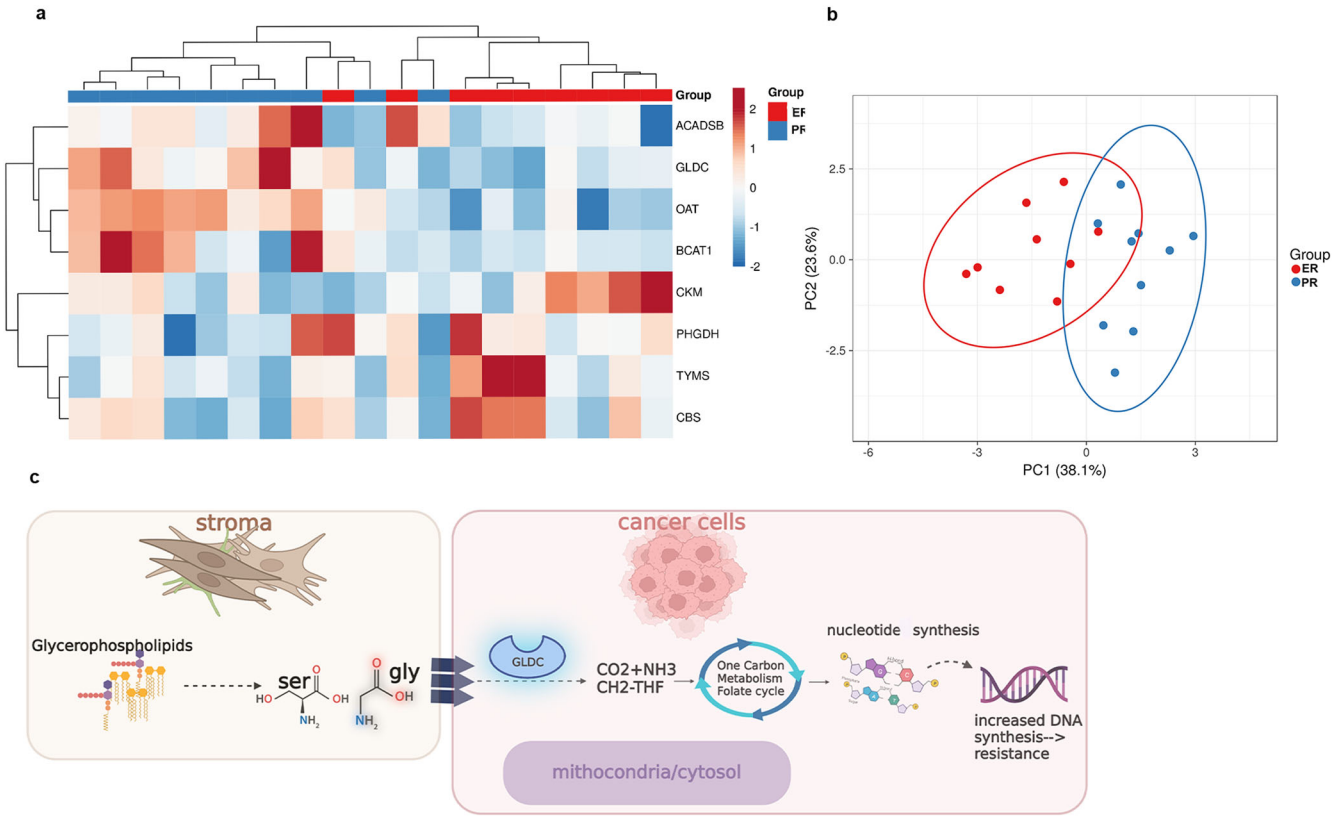

Fig. 5 Proteomic analysis of high-grade serous ovarian cancer (HGSC) samples obtained prior to neoadjuvant chemotherapy (NACT) based on excellent (ER) or poor (PR) response. a Unsupervised clustering of protein expression in ER and PR tissues. **b** PCA plot of the same features by case. **c** Proposed mechanism for the metabolic interactions between stroma and cancer cells. PCA principal component analysis, Ser serine, gly glycine, GLDC glycine decarboxylase. The results from the proteomics analyses shown in this figure were obtained from analysis performed on tumor tissue sections from pre-chemotherapy samples from 15 patients (7 ER and 8 PR). Differential analyses of global proteome or transcriptome matrixes were performed using LIMMA.

and interfering with the metabolism of aspartate and glycine. While the antibody-based targeting of phosphatidylserine has been shown in pre-clinical studies to overcome resistance to radiation and chemotherapy[33,34], the targeting of glycerophosphoserine has yet to be investigated. Interfering with aspartate and glycine metabolism could be done by blocking GLDC. GLDC, a mitochondrial enzyme, is part of a complex that oxidatively decarboxylates glycine[35]; high GLDC activity is strongly correlated with high rates of glutaminolysis and the synthesis of acetyl-CoA and fatty acids[36]. Notably, patients with HGSC with elevated GLDC levels have significantly worse PFS[37], a finding similar to that in patients with non-small cell lung cancer[30], in whom GLDC inhibition has been investigated in vitro and in vivo[38]. Combined treatment with GLDC inhibitors and platinum-based compounds, a completely novel strategy, might enhance sensitivity to chemotherapy in ovarian cancer. As mentioned above, and based on prior publications, glutaminolysis, and glutamine metabolism are part of the basis of reprogramming ovarian cancer cells towards increased proliferation and invasiveness[39]. Our study provides additional data on how the heterogeneous metabolism inside ovarian cancers might affect response to chemotherapy by promoting glycine-dependent nucleotide synthesis in cancer cells. However, additional work is needed to further test the biological importance of GLDC in ovarian and other cancers.

This study provides evidence that tumors with low sensitivity to NACT are characterized by different metabolic profiles, a finding that can be leveraged to stratify patients for treatment purposes. Additional research is needed to examine the therapeutic efficacy of targeting these differences. The availability of highly annotated tissues from patients undergoing standardized treatment and follow-up makes our results particularly relevant and translatable to the clinic. Future work will focus on the analysis of metabolomic and proteomics/phosphoproteomics profiles within an expanded cohort of tissues from patients with HGSC.

Our subgroup analysis was limited by the small sample size; therefore, a larger cohort and additional validation studies are needed. Tissue segmentation in stroma and epithelium was based on the morphological analysis of H&E-stained slides; additional subclassification of the TME with the identification of vessels, immune cell clusters, and different fibroblast subtypes is needed to further elucidate the metabolic changes in the stroma. Although MS imaging data provide spatially resolved molecular information, they are not quantitative; thus, the pathway analyses based on these data were exploratory in nature. Moreover, it should be noted that the predictive model was built from data extracted from tumor regions annotated by pathologic evaluation within the primary tissue types. As such, the model is limited to these tissue types and needs to be further expanded and validated for use in tissues in which higher degrees of cellular heterogeneity may influence the metabolic profiles.

METHODS

Patients

A total of 112 frozen samples from 59 patients were collected and analyzed with DESI-MS; these included pre-chemotherapy samples from 52 patients (30 ER and 22 PR) and post-chemotherapy samples from 37 patients (20 ER and 17 PR). Among these, frozen

tumor sections were retrieved from 48 patients from the MD Anderson Department of Gynecologic Oncology, 7 patients from the Gynecologic Cancer Translational Research Center of Excellence (GYN-COE) Program, and 4 patients from Washington University, St. Louis, as part of a collaborative study with the University of Iowa and MD Anderson Cancer Center. When available, two pre- or post-chemotherapy samples (one from adnexa and the other from a metastatic site such as the omentum, uterus, or abdominal organs) for each patient were collected and analyzed.

The collection of tissues from patients diagnosed and treated at the MD Anderson Cancer Center followed a specific algorithm: patients with suspected advanced primary ovarian cancer underwent surgical laparoscopy, during which their metastatic burden was assigned a modified Fagotti score[40,41] and their tissues obtained and stored. Following laparoscopy, patients with a predictive index value < 8 underwent primary reductive surgery, and patients with a predictive index value ≥ 8 underwent NACT followed by interval reduction surgery. After three to four cycles of carboplatin-based NACT (generally a paclitaxel- and carboplatin-based regimen), patients were considered "excellent responders" (ER) if there was a complete response or only microscopic disease left at time of interval surgery, or they were considered "poor responders" (PR) if they presented stable or progressive disease on radiologic evaluation and/or suboptimal interval cytoreduction after NACT, according to Response Evaluation Criteria in Solid Tumors version 1.1. At interval surgery, post-chemotherapy tissues were collected and stored. The study was approved by the Institutional Review Board of The University of Texas MD Anderson Cancer Center, and all samples were collected after obtaining written informed consent from patients.

For the collection of tissues from GYN-COE, frozen tumors and clinical data were collected before and after neoadjuvant paclitaxel and carboplatin chemotherapy from patients with histologically confirmed advanced-stage, high-grade serous ovarian or tubal carcinoma and banked at the Women's Health Integrated Research Center in Annandale, VA. These patients provided broad consent for their tissues to be used in future research under WCG IRB Protocol #20110222, Tissue and Data Acquisition Activity for the Study of Gynecologic Disease. The paired tumor specimens and clinical data were collaboratively evaluated under WCG IRB Protocol #14-1679, an Integrated Molecular Analysis of Endometrial Cancer, Ovarian Cancer, and Other Medical Conditions to Identify and Validate Clinically Informative Biomarkers and Factors, and the fully executed Material Transfer Agreement #205-20.

For the collection from Washington University, frozen tumors and clinical data were collected before neoadjuvant paclitaxel and carboplatin chemotherapy from patients with histologically confirmed advanced-stage, high-grade serous ovarian or tubal carcinoma and banked at the University of Iowa as part of a collaborative study; these patients gave informed consent as part of our Washington University Tumor Tissue Banking IRB 201105400 or our collaborative R01 with Iowa: IRB 201104242 and 20511102. The study was approved by the Institutional Review Board of the University of Iowa (protocol #201507805).

Unidentified frozen blocks from HGSC of two different patients were obtained from the Cooperative Human Tissue Network (CHTN) and used to test the reproducibility of DESI-MS on multiple sections (Supplementary Fig. 1).

In vivo models of ovarian cancer

Animal protocols were approved by the MD Anderson Institutional Animal Care and Use Committee and experiments were performed with 6- to 8-week-old female athymic nude mice (NCr-nude) obtained from Taconic Biosciences. Luciferase-labeled SKOV3ip1 ovarian cancer cells were used to establish xenograft models for all mouse experiments as described before[42]. Cells were cultured to 70–90% confluence and then trypsinized, washed twice with phosphate-buffered saline, and resuspended in ice-cold Hank's Balanced Salt Solution (cat. #21-021-CV; Cellgro). The mice were then inoculated with 1×10^6 SKOV3ip1 cells via intraperitoneal injection to the right side of the abdomen. Tumor establishment was subsequently confirmed after injection of 200 µL of 14.3 mg/mL luciferin (cat. #LUCK-1G; GoldBio) using a Xenogen IVIS in vivo imaging system. Following tumor establishments, mice were randomly assigned to treatment groups as described in {Glassman, 2023 #119}. For the purpose of this study, tumors from mice treated with vehicle control were considered. Investigators sacrificed the mice via carbon dioxide euthanasia followed by cervical dislocation once the mice were moribund. At the time of gross necropsy, mouse tumor weights, nodule numbers, distribution of metastasis, and presence of ascites were recorded. All tumor tissues were dissected, and samples were snap-frozen, fixed in formalin for paraffin embedding, or snap-frozen in optimal cutting temperature compound (Mercedes Scientific) for frozen slide preparation.

DESI-MS

A 2-dimensional Omni Spray (Prosolia Inc, Indianapolis, IN) was used for tissue imaging with an LTQ-Orbitrap Elite mass spectrometer (Thermo Scientific, San Juan, CA). DESI-MS imaging was performed in the negative ion mode from *m/z* 100 to 1500 with a hybrid mass spectrometer, which allows tandem MS experiments to be performed with high mass accuracy (<5 ppm mass error) and high mass resolution (60,000 resolving power). Imaging was performed using a spatial resolution of 200 µm. Ion images were assembled using Biomap (Novartis) software. For negative ion mode analyses, the histologically compatible spray solvent dimethylformamide:acetonitrile (DMF:ACN) 1:1 (v/v) was used to perform the imaging analyses at a flow rate of 1.2 µL/min[38]. DESI-MS data were deposited at https://data.mendeley.com/datasets/zzr5rk7vj5/1. For many cases we analyzed multiple sections of the same tumor; prior studies have evaluated the reproducibility of DESI-MS imaging on serial tissue sections[43].

Histopathology and light microscopy

The same tissue sections analyzed by DESI-MS were then subjected to standard H&E staining. Pathologic diagnosis was made by Dr. Jinsong Liu using light microscopy. Light microscopy images were obtained and subjected to manual tissue segmentation into the two regions of interest, epithelium, and stroma, based on morphologic assessment.

DESI-MS reproducibility

In order to test the reproducibility of DESI-MS on several sections from the same tumor block, we used sections from frozen tumor blocks derived from two patients with ovarian cancer and 5 total ovarian cancer xenograft mice. Two sections from each human tumor and four sections from four of the five xenografts were used for the analysis. For one of the five xenografts two sections were analyzed. After DESI-MS, mass spectra were identified, and a Cosine Similarity analysis was performed. (Supplementary Fig. 1).

Global proteomics and phosphoproteomics analysis

Global proteomics and phosphoproteomics analysis of pre-chemotherapy samples from 7 ER and 8 PR patients, including tumors from primary and metastatic disease sites for a subset of cases, was performed as described previously[13]. Briefly, laser microdissection was used to collect whole tumor samples (cancer and stromal cells combined), which underwent pressure-assisted digestion employing a barocycler (2320EXT Pressure BioSciences, Inc.) and a heat-stable form of trypsin (SMART Trypsin,

ThermoFisher Scientific, Inc.). Peptide digestion was labeled per tandem mass tag channel (TMT-11, ThermoFisher Scientific, Inc.). Sample multiplexes were separated offline using basic reversed-phase liquid chromatographic fractionation on a 1260 Infinity II liquid chromatograph (Agilent) into 96 fractions using a linear gradient of acetonitrile (0.69% min) followed by concatenation (36 total fractions for global proteomics and 12 fractions for phosphopeptides serially enriched by TiO2 and Fe-IMAC). Each pooled fraction was resuspended in 100 mM NH4HCO3 and analyzed by LC-MS/MS employing a nanoflow LC system (EASY-nLC 1200, ThermoFisher Scientific) coupled online with an Orbitrap Fusion Lumos Tribrid mass spectrometer (ThermoFisher Scientific). In brief, each fraction was loaded onto a nanoflow HPLC system fitted with a reversed-phase trap column (Acclaim PepMap100 C18, 20 mm, nanoViper, Thermo Scientific) and a heated (50 °C) reversed-phase analytical column (Acclaim PepMap RSLC C18, 2 µm, 100 Å, 75 µm × 500 mm, nanoViper, Thermo Fisher Scientific) coupled online with the mass spectrometer. Peptides were eluted using a linear gradient of 2% mobile phase B (95% acetonitrile, 0.1% formic acid) to 32% mobile phase B over 120 min at a constant flow rate of 250 nL/min. High-resolution (R = 60,000 at m/z 200) broadband (m/z 400-1600) mass spectra were acquired, followed by the selection of the 12 most intense molecular ions in each MS scan for high-energy collisional dissociation. Global protein-level and phosphosite identifications were generated by searching .raw data files with a publicly available, non-redundant human proteome database (Swiss-Prot, Homo sapiens [http://www.uniprot.org/]) using Mascot (Matrix Science), Proteome Discoverer (Thermo Fisher Scientific), and in-house tools using identical parameters as described previously[34]. Differential analyses of global proteome or transcriptome matrixes were performed using the LIMMA package (version 3.8) in R (version 3.5.2), and candidates mapping to metabolomic pathways of interest identified from the Reactome databases were prioritized for downstream analysis. A more detailed description of this method can be found in[13]. A total of 7148 proteins and >1075 phosphosites were co-quantified across cases (Supplemental Tables 13–18). Protein and phosphosite mapping to the Reactome pathways altered between ER and PR cases observed in the metabolomic analysis were selected for further analysis. Pathways with the highest number of proteins quantified included the metabolism of amino acids and derivatives, metabolism of nucleotides, and respiratory electron transport and related pathways. Differential analysis revealed that most proteins and phosphosites were significantly altered (LIMMA $p < 0.05$, ±1.5-fold change) between the PR and ER cases mapped to the metabolism of amino acids and derivatives and metabolism of nucleotide pathways. A heatmap for the eight proteins significantly altered in PR versus ER pre-chemotherapy tumors, mostly mapping to the metabolism of amino acids and derivatives pathway (z-score = 0.728 p-value 1.69E-13, derived from Ingenuity Pathway Analysis), is shown in Fig. 5a. A principal component analysis plot of these proteins by case (Fig. 5b) illustrates a distinct separation of the pre-chemotherapy PR and ER tumors. For the phosphoproteome analysis, the comparison reflects the relative abundance of a given phosphosite, i.e., phosphorylated residue, of interest in one condition versus the other. The mass spectrometry proteomics data are available at the ProteomeXchange Consortium via the PRIDE (https://doi.org/10.1093/nar/gky1106) partner repository with the dataset identifier PXD014980.

Quantification

MS data were extracted from the regions of interest using MSiReader software. Significance analysis of microarrays was used to identify ions with significantly different abundances in ER samples compared with PR samples and in pre-chemotherapy samples compared with post-chemotherapy samples. Features below 10% FDR were selected. Selective analyses were carried out separately for data extracted from epithelial and stromal regions. The identified metabolites were divided for analytical purposes into non-lipid (such as uracil, fumarate, hypoxanthine, glutamic acid, and citrate) and lipid (such as fatty acids, glycolipids, ceramides, and cardiolipins) categories.

Pathway analysis

To study the non-lipid metabolic species, we carried out pathway analyses using REACTOME (https://reactome.org/) and confirmed the findings in Pathway Studio (https://www.pathwaystudio.com/). Enriched REACTOME pathways were ordered according to a probability score corrected for FDR using the Benjamini-Hochberg method. We selected the 10 most relevant pathways in REACTOME sorted by p-value, and pathways with a common hit in Pathway Studio were considered. Pathway analysis was performed only when at least two metabolites (small molecules) were recognized by the software. In cases in which one software was not able to recognize more than two metabolites, the results from the other software were considered.

Prediction model

The glmnet package[44] in R version 3.6.3 was used to create a ridge regression model for the classification of treatment response. Prior to analysis, data were pre-processed by removing m/z values that were present in less than 10% of all spectra. Intensities were median-normalized by dividing the intensity of each individual ion in a spectrum by the median intensity for the same spectrum. Ten-fold cross-validation was used to create a ridge regression model for the classification of ER and PR samples from the epithelial regions of pre-chemotherapy tumor tissues. The analysis was restricted to the primary sites (adnexa and ovaries), and samples from metastatic sites (omentum or abdominal organs) were excluded. The ridge regression model used 78 features for class distinction, represented by a variety of small molecules and lipid species between 100 and 1000 m/z. The ridge regression model was used to estimate the probability of every mass spectrum belonging to either the ER or PR group. If more than 50% of the spectra were correctly predicted for a single sample, we considered the sample to be correctly classified in our per-sample prediction results. Pixel-based and sample-based accuracies, sensitivities, and specificities were calculated.

Sparse partial least squares discriminant analysis

Metaboanalyst 5.0 was used for sparse partial least squares discriminant analysis (sPLS-DA). Prior to sPLS-DA, data were TIC-normalized and mean-centered. sPLS-DA plots were used to visualize the distinct separation between pre- and post-chemotherapy samples in both the ER samples and PR samples (Fig. 3b).

Reporting summary

Further information on research design is available in the Nature Research Reporting Summary linked to this article.

DATA AVAILABILITY

This study did not generate new unique reagents. Further information and requests for resources and reagents should be directed to and will be fulfilled by the lead contacts, Anil K. Sood (asood@mdanderson.org) and Livia S. Eberlin (Livia.Eberlin@bcm.edu). The MS proteomics data are available at the ProteomeXchange Consortium via the PRIDE (https://doi.org/10.1093/nar/gky1106) partner repository with the dataset identifier PXD014980. DESI-MS data were deposited at https://data.mendeley.com/datasets/zzr5rk7vj5/1.

CODE AVAILABILITY

The glmnet package in R[44] was used to create a ridge regression model for the classification of treatment response. Metaboanalyst 5.0 was used for sparse partial least squares discriminant analysis (sPLS-DA).

Received: 18 October 2022; Accepted: 26 September 2023;
Published online: 03 November 2023

REFERENCES

1. Piccart, M. J. et al. Long-term follow-up confirm's a survival advantage of the paclitaxel-cisplatin regimen over the cyclophosphamide-cisplatin combination in advanced ovarian cancer. *Int J. Gynecol. Cancer* **13**, 144–148 (2003).
2. Siegel, R. L., Sahar, L., Portier, K. M., Ward, E. M. & Jemal, A. Cancer death rates in US congressional districts. *Ca-Cancer J. Clin.* **65**, 339–344 (2015).
3. Fleming, N. D. et al. Laparoscopic surgical algorithm to triage the timing of tumor reductive surgery in advanced ovarian cancer. *Obstet. Gynecol.* **132**, 545–554 (2018).
4. Chughtai, S. et al. A multimodal mass spectrometry imaging approach for the study of musculoskeletal tissues. *Int J. Mass Spectrom.* **325**, 150–160 (2012).
5. Norris, J. L. & Caprioli, R. M. Analysis of tissue specimens by matrix-assisted laser desorption/ionization imaging mass spectrometry in biological and clinical research. *Chem. Rev.* **113**, 2309–2342 (2013).
6. Eberlin, L. S. et al. Classifying human brain tumors by lipid imaging with mass spectrometry. *Cancer Res* **72**, 645–654 (2012).
7. Eberlin, L. S. et al. Molecular assessment of surgical-resection margins of gastric cancer by mass-spectrometric imaging. *P Natl Acad. Sci. USA* **111**, 2436–2441 (2014).
8. Guenther, S. et al. Spatially resolved metabolic phenotyping of breast cancer by desorption electrospray ionization mass spectrometry. *Cancer Res* **75**, 1828–1837 (2015).
9. Venter, A., Sojka, P. E. & Cooks, R. G. Droplet dynamics and ionization mechanisms in desorption electrospray ionization mass spectrometry. *Anal. Chem.* **78**, 8549–8555 (2006).
10. Wiseman, J. M., Ifa, D. R., Song, Q. Y. & Cooks, R. G. Tissue imaging at atmospheric pressure using desorption electrospray ionization (DESI) mass spectrometry. *Angew. Chem. Int Ed.* **45**, 7188–7192 (2006).
11. Sans, M. et al. Metabolic markers and statistical prediction of serous ovarian cancer aggressiveness by ambient ionization mass spectrometry imaging. *Cancer Res* **77**, 2903–2913 (2017).
12. Cao, K. A. L., Boitard, S. & Besse, P. Sparse PLS discriminant analysis: biologically relevant feature selection and graphical displays for multiclass problems. *Bmc Bioinformatics*. **12**, https://doi.org/10.1186/1471-2105-12-253 (2011).
13. Lee, S. et al. Molecular analysis of clinically defined subsets of high-grade serous ovarian cancer. *Cell Rep.* **31**, https://doi.org/10.1016/j.celrep.2020.03.066 (2020).
14. van Gastel, N. et al. Induction of a timed metabolic collapse to overcome cancer chemoresistance. *Cell Metab.* **32**, 391 (2020).
15. Nieman, K. M. et al. Adipocytes promote ovarian cancer metastasis and provide energy for rapid tumor growth. *Nat. Med* **17**, 1498–U1207 (2011).
16. Colegio, O. R. et al. Functional polarization of tumour-associated macrophages by tumour-derived lactic acid. *Nature* **513**, 559 (2014).
17. Desbats, M. A., Giacomini, I., Prayer-Galetti, T. & Montopoli, M. Metabolic plasticity in chemotherapy resistance. *Front Oncol.* **10**, https://doi.org/10.3389/fonc.2020.00281 (2020).
18. Fox, D. B. et al. NRF2 activation promotes the recurrence of dormant tumour cells through regulation of redox and nucleotide metabolism. *Nat. Metab.* **2**, 318 (2020).
19. Goetze, K., Walenta, S., Ksiazkiewicz, M., Kunz-Schughart, L. A. & Mueller-Klieser, W. Lactate enhances motility of tumor cells and inhibits monocyte migration and cytokine release. *Int J. Oncol.* **39**, 453–463 (2011).
20. Vegran, F., Boidot, R., Michiels, C., Sonveaux, P. & Feron, O. Lactate influx through the endothelial cell monocarboxylate transporter MCT1 supports an NF-kappa B/IL-8 pathway that drives tumor angiogenesis. *Cancer Res.* **71**, 2550–2560 (2011).
21. Rothberg, J. M. et al. Acid-mediated tumor proteolysis: contribution of cysteine cathepsins. *Neoplasia* **15**, 1111–1123 (2013).
22. Nyen, T. V. et al. Serine metabolism remodeling after platinum-based chemotherapy identifies vulnerabilities in a subgroup of resistant ovarian cancers. *Nat. Commun.* **13**, https://doi.org/10.1038/s41467-022-32272-6 (2022).
23. Yang, L. F. et al. Targeting stromal glutamine synthetase in tumors disrupts tumor microenvironment-regulated cancer cell growth. *Cell Metab.* **24**, 685–700 (2016).
24. Pavlova, N. N. et al. As extracellular glutamine levels decline, asparagine becomes an essential amino acid. *Cell Metab.* **27**, 428 (2018). -+.
25. Zhang, J. et al. Asparagine plays a critical role in regulating cellular adaptation to glutamine depletion. *Mol. Cell* **56**, 205–218 (2014).
26. Kopp, F. et al. The glycerophospho metabolome and its influence on amino acid homeostasis revealed by brain metabolomics of GDE1(−/−) Mice. *Chem. Biol.* **17**, 831–840 (2010).
27. Kume, A. et al. The glycine cleavage system - molecular-cloning of the chicken and human glycine decarboxylase Cdnas and some characteristics involved in the deduced protein structures. *J. Biol. Chem.* **266**, 3323–3329 (1991).
28. Bhatia, M. et al. Allosteric inhibition of MTHFR prevents futile SAM cycling and maintains nucleotide pools in one-carbon metabolism. *J. Biol. Chem.* **295**, 16037–16057 (2020).
29. Tibbetts, A. S. & Appling, D. R. Compartmentalization of mammalian folate-mediated one-carbon metabolism. *Annu. Rev. Nutr.* **30**, 57–81 (2010).
30. Zhang, W. C. et al. Glycine decarboxylase activity drives non-small cell lung cancer tumor-initiating cells and tumorigenesis (vol 148, pg 259, 2012). *Cell* **148**, 1066–1066 (2012).
31. Liu, R. et al. mTORC1 activity regulates post-translational modifications of glycine decarboxylase to modulate glycine metabolism and tumorigenesis. *Nat. Commun.* **12**, https://doi.org/10.1038/s41467-021-24321-3 (2021).
32. Knox, R. J., Friedlos, F., Lydall, D. A. & Roberts, J. J. Mechanism of cytotoxicity of anticancer platinum drugs - evidence that Cis-Diamminedichloroplatinum(Ii) and Cis-Diammine-(1,1-Cyclobutanedicarboxylato)Platinum(Ii) differ only in the kinetics of their interaction with DNA. *Cancer Res.* **46**, 1972–1979 (1986).
33. Budhu, S. et al. Targeting phosphatidylserine enhances the anti-tumor response to tumor-directed radiation therapy in a preclinical model of melanoma. *Cell Rep.* **34**, 108620 (2021).
34. Schad, S. et al. Phosphatidylserine targeting antibody enhances anti-tumor activity of adoptive cell therapies in a mouse melanoma model. *J. Immunol.* **204** (2020).
35. Hiraga, K. & Kikuchi, G. The mitochondrial glycine cleavage system - functional association of glycine decarboxylase and aminomethyl carrier protein. *J. Biol. Chem.* **255**, 1671–1676 (1980).
36. Alptekin, A. et al. Glycine decarboxylase is a transcriptional target of MYCN required for neuroblastoma cell proliferation and tumorigenicity. *Oncogene* **38**, 7504–7520 (2019).
37. Gyorffy, B., Lanczky, A. & Szallasi, Z. Implementing an online tool for genome-wide validation of survival-associated biomarkers in ovarian-cancer using microarray data from 1287 patients. *Endocr.-Relat. Cancer* **19**, 197–208 (2012).
38. Woo, C. C., Kaur, K., Chan, W. X., Teo, X. Q. & Lee, T. H. P. Inhibiting glycine decarboxylase suppresses pyruvate-to-lactate metabolism in lung cancer cells. *Front. Oncol.* **8**, https://doi.org/10.3389/fonc.2018.00196 (2018).
39. Han, C., Lu, X. B. & Nagrath, D. Regulation of protein metabolism in cancer. *Mol Cell Oncol.* **5**, https://doi.org/10.1080/23723556.2017.1285384 (2018).
40. Fagotti, A. et al. A laparoscopy-based score to predict surgical outcome in patients with advanced ovarian carcinoma: a pilot study. *Ann. Surg. Oncol.* **13**, 1156–1161 (2006).
41. Hansen, J. M. et al. Concordance of a laparoscopic scoring algorithm with primary surgery findings in advanced stage ovarian cancer. *Gynecol. Oncol.* **151**, 428–432 (2018).
42. Glassman, D. et al. Exploiting metabolic vulnerabilities after anti-VEGF antibody therapy in ovarian cancer. *Iscience.* **26**, https://doi.org/10.1016/j.isci.2023.106020 (2023).
43. Dill, A. L., Eberlin, L. S., Costa, A. B., Ifa, D. R. & Cooks, R. G. Data quality in tissue analysis using desorption electrospray ionization. *Anal. Bioanal. Chem.* **401**, 1949–1961 (2011).
44. Friedman, J., Hastie, T. & Tibshirani, R. Regularization paths for generalized linear models via coordinate descent. *J. Stat. Softw.* **33**, 1–22 (2010).

ACKNOWLEDGEMENTS

This work was supported in part by the MD Anderson Ovarian Cancer Moon Shot; CPRIT (RP180381); the National Institutes of Health (CA217685 [Ovarian Cancer SPORE], CA193249, CA209904, and CA193249-S1); the Ovarian Cancer Research Alliance; the American Cancer Society; the Dunwoody Fund; the Le Bert Suess Family Endowment for Ovarian Cancer Research; the Frank McGraw Memorial Chair in Cancer Research; the Foundation for Women's Cancer; the Amy Krouse Rosenthal Foundation; and Judy's Mission to End Ovarian Cancer Foundation (Research Grant for Early Detection of Ovarian Cancer). Y.W is supported in part by Department of Defense Ovarian Cancer Research Program (W81XWH-20-1-0335). We acknowledge the Research Medical Library at MD Anderson Cancer Center for editing the text. For the GYN-COE collection, the collection and banking of these specimens and data were funded by awards HU0001-16-2-0006, HU0001-19-2-0031, HU0001-20-2-0033, and HU0001-21-2-0027 from the Uniformed Services University of the Health Sciences from the Defense Health Program to the Henry M. Jackson Foundation for the Advancement of Military Medicine, Inc., Gynecologic Cancer Center of Excellence Program (PI: Yovanni Casablanca, Co-PI: G. Larry Maxwell). We acknowledge BioRender for figure composition.

AUTHOR CONTRIBUTIONS

S.C.: Project administration, writing original draft and review/editing, supervision. P.L.L.: Software suggestion. J.L.: Validation. S.B., M.S., M.K., I.P., Y.W., N.W.B., W.B., T.P.C., L.G.M.: Formal analysis and data curation. S.B., M.S., M.K., I.P., N.W.B., W.B., T.P.C., L.G.M., P.L.L., S.K.L., P.H.T., M.J.G., J.L., S.L., L.S.E., A.K.S., K.M.D.: Review/editing of the text. K.I.F., E.S., E.B., Y.W.: Revision/editing of the text. S.C., S.L., L.S.E., A.K.S.: Investigation. S.C., L.S.E., A.K.S.: Conceptualization. S.C., E.S., E.B.: Visualization. S.C., K.I.F.: Data curation. K.M.D., S.K.L., P.H.T., M.J.G.: Provision of study material (patients/laboratory samples). N.W.B., T.P.C., L.G.M.: Funding aquisition. L.S.E., A.K.S.: Methodology, resources, funding.

COMPETING INTERESTS

N.F. declares that she is a consultant for GSK and Immunogen. L.S.E. declares that she receives funding from Thermo Fisher, Merck & Co, Waters corporation, and Eli Lilly and has stocks in MS Pen Technologies. A.K.S. declares that he is a shareholder of BioPath, and is a consultant for Merck, AstraZeneca, Onxeo, ImmunoGen, Ivlon, GSK, and Kiyatec. The remaining authors declare no competing financial or non-financial interests.

ADDITIONAL INFORMATION

Supplementary information The online version contains supplementary material available at https://doi.org/10.1038/s41698-023-00454-0.

Correspondence and requests for materials should be addressed to Livia S. Eberlin or Anil K. Sood.